# Extraction of periodic signals in GNSS vertical coordinate time series using adaptive Ensemble Empirical Modal Decomposition method

Weiwei Li[1], Jing Guo[1]

[1] College of Geodesy and Geomatics, Shandong University of Science and Technology, Qingdao, 266590, China

*Correspondence to*: Weiwei Li (whereareou@126.com)

**Abstract.** ~~Ensemble Empirical Mode Decomposition (EEMD) has been widely used in the data analysis.~~ Empirical Modal Decomposition（EMD) is an efficient tool of extracting signal from stationary or non-stationary time series, which is enhanced in the stability and robustness by Ensemble Empirical Mode Decomposition (EEMD). Adaptive EEMD further improves computational efficiency through the adaptability in the white noise amplitude and set average number. However, its effectiveness of the periodic signal extraction in Global Navigation Satellite System (GNSS) coordinate time series regarding on the inevitable missing data and offsets issues have not been comprehensively validated. ~~It is verified with 5-year time series through 300 simulations for each case.~~ In order to thoroughly investigate their impacts, we simulated 5 years of daily time series data with different missing data percentage or different number of offsets and conducted 300 times for each simulation. The results show that high accuracy could reach for the overall random missing rate below 15% and avoiding consecutive missing ~~epochs~~ exceeding 30 days. Meanwhile, offsets should be corrected in advance regardless of their magnitudes. The analysis of vertical component of 13 stations within the Australian Global Sea Level Observing System (GLOSS) monitoring network~~,~~ demonstrates the advantage ~~in~~ of adaptive EEMD in revealing the time-varying characteristics of periodic signals. From the perspectives of correlation coefficients (CC), root mean square error (RMSE), power spectral density ~~(PSD)~~ indices ($\kappa$) and ~~signal noise ratio~~ signal-to-noise (SNR), the means for adaptive EEMD are 0.36, 0.81, -0.18 and 0.48, respectively, while for least squares (LS), they are 0.27, 0.86, -0.50 and 0.23. Meanwhile, significance test of the residuals further ~~substantiate~~ substantiates the effectiveness in periodic signal extraction, which shows there is no annual signal remained. Also, the longer the series, the higher the accuracy of extracted periodic signal is reasonable concluded via the significance test. ~~Furthermore, the time-varying periodic characteristics is more conducive to analyze the driving factors.~~ Moreover, driving factors is more effectively facilitated by the time-varying periodic characteristics compared with the constant periodic signal derived by LS. Overall, the application of adaptive EEMD could achieve high accuracy in analyzing GNSS time series, but it should be based on the proper dealing with missing data and offsets.

## 1 Introduction

With the development of GNSS (Global Navigation Satellites Systems), international GNSS service (IGS) and many countries have established GNSS networks, such as the worldwide IGS, SAPOS (the satellite positioning service of the German National Survey) in Germany, GEONET (GNSS Earth Observation Network system) in Japan, CMONOC (Crustal Movement Observation Network of China) in China. Also, there is a GNSS data center named SONEL (Système d'Observation du Niveau des Eaux Littorales), which serves the Global Sea Level Observing System (GLOSS). These GNSS networks are widely applied in geodesic and geodynamics studies (Gülal et al., 2013; Scaramuzza et al., 2017). ~~Global Navigation Satellite System (~~GNSS~~)~~ coordinate time series are a crucial type of geophysical data. They can not only be used to obtain accurate positions and velocities of stations ~~(Blewitt and Lavallée, 2002)~~ (Johnson et al., 2021; Zhou et al., 2022), but also for better studying Earth’s dynamic processes such as crustal movement ~~(Manevich et al., 2021)~~ (Calais et al., 2023), post-ice rebound and sea level change (~~Md~~ Din et al., 2019), inversion mass change (Willen et al., 2022), and ~~so on~~ other applications (Dong et al., 2002; Munekane, 2021; Costantino et al., 2023). ~~From these data, we can observe significant periodic variations in addition to long-term trends and noise.~~ These coordinate time series are generally decomposed of periodic signal, trends and noise. ~~These~~ The periodic ~~variations~~ signals are caused by a complex interplay of the Earth’s own physical properties and environmental factors, which is particularly obvious in the elevation direction (~~Davis et al., 2012; Jiang et al., 2013;~~ Dong et al., 2002; Ray et al., 2008; Wang et al., 2018). The trend terms are composed with long-term trend and transient trend. For the transient trend, it mainly includes the effect of earthquake and tide. For the 26 December 2004 Sumatra earthquake ($M_w$ 9.2–9.3) caused the afterslip of larger than 10 mm within minutes as far away as India (Blewitt et al., 2006). It is usually modelled with logarithmic or exponential functions (Hetland and Hager, 2006; Nishimura, 2014; Tobita, 2016). Moreover, modulations in plate motion compatible with the Solar year, the period of the Lunar perigee and Lunar nodes, which clearly the influence of lunar and solar tidal forces on the plate motion (Zaccagnino et al., 2020). Also, this motion by oscillating tide can be evidenced by the deep tremors (Ide and Tanaka., 2014). Since our focus is the long-term trend, we mainly investigate the impact of periodic signals on it. Therefore, accurately extracting periodic signals from GNSS coordinate time series ~~holds significant importance~~ is crucial (Van Dam et al., 2001; Sorin et al., 2021). However, ~~in previous studies,~~ the periodic signals ~~extracted~~ estimated by the ~~commonly used LS~~ traditional least squares (LS) method did not agree well with the actual periodic variations (Bennett, 2008; Li, 2020). Therefore, ~~many~~ some scholars have ~~conducted studies on~~ aimed at more suitable periodic signal extraction methods, ~~some of which include~~ The Kalman filtering, assuming signals random, ~~which~~ is contrary to the real GNSS time series containing power-law noise (Davis et al., 2012). Also, the high sensitivity of F-test detection to noise may lead to the incorrect determination of the presence of periodic signals (Li and Shen, 2014). The Principal Component Analysis (PCA) method found that most GNSS stations around the world have a nonlinear periodic pattern, with annual and semi-annual terms dominating ~~(Zhang et al., 2019)~~ (Shen et al., 2014). These studies verified the existence of time-varying ~~amplitude~~ periodic signals in GNSS time series and separated the signals according to different methods. ~~However, the accurate extraction of tectonic motion information containing various noise,~~

~~errors and non-tectonic periodic signals from actual observation still necessitates the continuous exploration of novel approaches and methods.~~

Moreover, Empirical Mode Decomposition (EMD) introduced by Huang et al (Huang et al., 1998) is initially focused on the analysis of signals that are a mixture of harmonic oscillations with different periods. EMD requires the construction of the upper and lower envelopes based on the local extrema, through which approximating curves are drawn using cubic splines (Kopsinis and McLaughlin, 2008). Because of this, it works unstably once local extrema are poorly defined, for example, when the data contain relatively long plateaus of constant values or short-lived waves of small amplitude and short period (Huang et al., 2009). Adding white noise to the original data could create auxiliary local extrema, which regularizes the determination of the Intrinsic Mode Functions (IMFs) sequence, and the subsequent averaging sharply reduces the influence of white noise due to their independence (Wu and Huang, 2009). This is the feature of Ensemble Empirical Mode Decomposition (EEMD). However, the selection of empirical white noise magnitude and set average number may vary from person to person. Due to the adaptivity in the two variables, this paper employs an adaptive Ensemble Empirical Mode Decomposition (EEMD) method in GNSS coordinate time series analysis. ~~This paper employs an adaptive Ensemble Empirical Mode Decomposition (EEMD) method for signal decomposition capable of decomposing nonlinear and nonstationary signals into multiple physically well-defined Intrinsic Mode Functions (IMFs) with amplitude-varying characteristics over time (Xu, 2022).~~ The adaptive ~~Adaptive~~ EEMD has significant advantages in terms of noise immunity, avoidance of local extremes, stability of IMFs, ~~avoidance of local extremes,~~ adaptivity and consistency ~~of results~~ (Liu et al., 2023). It is suitable for signal components of different scales and frequencies, which improves the stability and reliability of decomposition ~~(Wu and Huang, 2009)~~. ~~This method is widespread in data processing. However, there are some limitations, such as high requirements of the completeness of the time series (Agnieszka and Dawid, 2022), and~~ Nevertheless, it has high requirements on data completeness (Agnieszka and Dawid, 2022). Besides, offsets which usually occur in GNSS coordinate time series have not yet been comprehensively ~~assessed.~~ included in the application of adaptive EEMD.

~~The trend in vertical direction of GNSS stations nearby the tide gauges is essential in obtaining the absolute sea level.~~ To obtain the absolute sea level from the tide gauges, their vertical trend should be removed, which can be measured by GNSS stations nearby the tide gauges. The GNSS stations belong to SONEL aim at providing high precision continuous monitoring. However, the trend is affected by the periodic signals contained in GNSS time series (Bos et al., 2010; Klos et al., 2018). Therefore, it is of paramount significance to get the periodic signal of high accuracy. ~~for the stations belong to SONEL (Système d'Observation du Niveau des Eaux Littorales), which serves as the GNSS data center for the Global Sea Level Observing System. Therefore, this~~ This paper applies adaptive EEMD to the periodicity assessment of 13 Australian stations in ~~GLOSS~~ SONEL. Section 2 describes the principles in detail, Section 3 verifies its effectiveness in synthetic time series, and 300 simulations were conducted for each of the experiments in the focused missing data and offset issues. The practical analysis ~~of~~ for the selected 13 stations located in Australia ~~in GLOSS~~ are carried out in Sect. 4, and the conclusions are summarized ~~in Sect. 5~~ in the last one.

## 2 Principle and Method

Due to the uncertain quantity of IMFs, there may be issues of frequency overlap and mode mixing among different IMFs, which can affect the decomposition and analysis of ~~Empirical Modal Decomposition (~~EMD~~)~~ signals (Huang et al., 1999). The employed EEMD method effectively mitigates the impact of mode mixing phenomena, enhancing the precision and robustness of signal decomposition ~~(Zhang et al., 2009)~~ (Agnieszka and Dawid, 2022). This method ~~is to add~~ consists in adding white noise to the original signal and uses the uniform distribution of Gaussian noise to alter the distribution of extreme points, ensuring signal continuity within each frequency band. Subsequently, the components of the multiple decomposed IMFs are averaged to mitigate the impact of random noise ~~(Huang et al., 1917; Yi et al., 2022)~~ (Huang et al., 1998). The specific steps are as follows (Peng et al., ~~1971~~2018; Liu et al., 2023)~~:~~,

Step 1: Add the same length Gaussian white noise sequence to the data $x(t)$ multiple times.

$$X_i(t) = x(t) + u \cdot a_i(t)\ , \tag{1}$$

Where $u$ is the ~~amplitude coefficient~~ magnitude of the added white noise~~ added~~, and $a_i(t)$ is the white noise added for the $i$th time, ~~where $i = 1,2,\ldots,m,\ t = 1,2,\ldots,T$.~~ where $t = 1,2,\ldots,T$, $i = 1,2,\ldots,m$, $m$ is set average number.

Step 2: Decompose the~~ original~~ signal $X_i(t)$ with noise to obtain the IMF components ~~of each order~~ by EMD.

$$X_i(t) = \sum_{j=1}^{n} c_{i,j}\,(t) + r_{i,n}(t)\ , \tag{2}$$

Where $c_{i,j}$ is the $j$th IMF of EMD decomposition with white noise added for the $i$th time, and $r_{i,n}$ is the remainder after decomposition.

Step 3: Calculate the mean value of the corresponding IMF component obtained from each decomposition, to get the final IMF component of EEMD.

$$IMF_j(t) = \frac{1}{m}\sum_{i=1}^{m} c_{i,j}\,(t)\ , \tag{3}$$

Where $IMF_j(t)$ is the $j$th IMF component obtained after EEMD decomposition of the decomposed signal.

~~However, two parameters in Step 1~~ We can see those two variables (added white noise amplitude $u$ and set average number $m$) in ~~EEMD~~ Step 1 are crucial, which directly affect the EEMD decomposition. For ~~the~~ too large white noise, it can mask the real signal. For ~~the~~ tiny white noise, its modal effect is not obvious. The larger the set average number, the smaller the decomposition error, ~~but the increase will reduce the computational efficiency.~~ however, it leads to a reduction in computational efficiency. Therefore, it is ~~important~~ key to balance both white noise amplitude and set average number, which represents the adaptivity in EEMD (Liu et al., 2023). The adaptive EEMD method can avoid ~~a large number of parameters~~ setting variables manually and ~~significantly~~ greatly improve decomposition efficiency and accuracy. However, the adaptive EEMD still suffers from boundary effects, which refers the problem of unstable or distorted decomposition due to the lack of extreme points at the end. In this paper, it is mitigated by ~~using~~ the extreme value extension method ~~(Qi et al., 2003)~~ (Wu and Qu, 2008).

~~While, the preprocessing is also essential for EEMD application. This involves selection of enough observations in good continuity, outliers removing, offset detection and missing data filling.~~ While preprocessing is also essential for adaptive EEMD application, which involves the selection of good continuity and sufficient data, outliers removing, offset detection and missing data filling. Here, the robust IQR method is used for outlier removal ~~(Shu, 2021)~~ (He et al., 2017) and Iterative Empirical Mode Decomposition (IEMD) is utilized for missing data filling (Qiu et al., 2022). The specific IEMD algorithm is seen in Fig. 1. ~~All the missing epochs are initialized with the mean value of the observed epochs to construct a new complete time series $x'(t)$.~~ All the missing data are firstly filled with the mean of the observed data to construct an initial complete time series $x'(t)$. Subsequently, traditional EMD decompose $x'(t)$ into a series of IMF components with frequency from high to low and one residual term. Generally, ~~the boundary IMF component is determined by using correlation coefficient criterion during the process of noise reduction (Jia et al., 2015). When the correlation coefficient between the IMF component and the time series $x'(t)$ reaches the minimum value for the first time, the corresponding IMF component is the boundary, with $k$ representing the boundary index.~~ the boundary IMF index $k$ is determined by correlation coefficient between the IMF component and the time series $x'(t)$ (Wang et al., 2023), at which reaches the minimum value for the first time. Then the signals $\hat{x}'(t)$ are reconstructed by summing the IMF components after the boundary IMF component and residual term. The ~~epochs of~~ missing data are ~~replaced~~ updated by the corresponding part of reconstructed signals $\hat{x}'(t)$. When the difference of missing data $|\Delta x'(t)_{miss}|$ between two iterations is smaller than $\varepsilon$, the iterative process is terminated, resulting in the final complete time series. Otherwise, the iteration continues. $\varepsilon$ represents a threshold (0.005 in this paper) to terminate the iteration process.

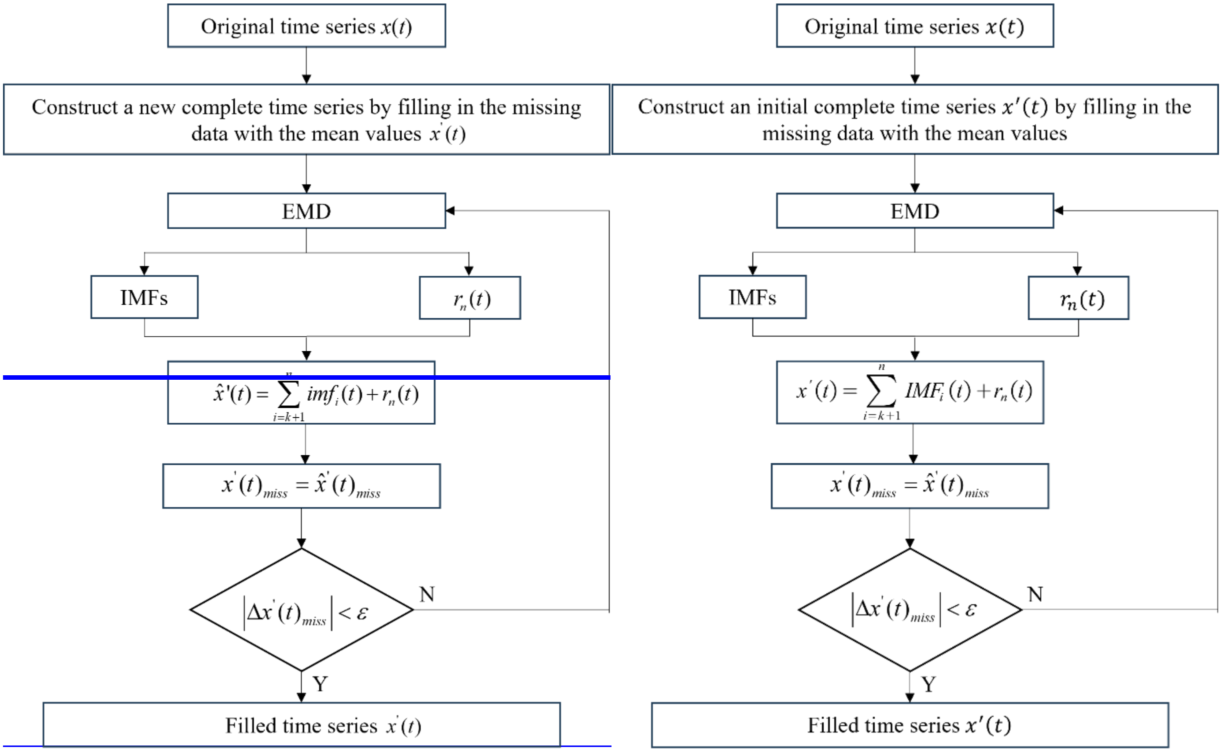


**Figure 1: Flow chart of IEMD for filling.**

With the complete data, the periodic signals can be extracted using adaptive EEMD method. Firstly, the time series are decomposed into multiple IMFs and corresponding residuals. Secondly, the high-frequency and low-frequency IMFs are determined by the energy value method ~~(Zheng, 2021)~~ (Cheng et al., 2006). Thirdly, the Lomb spectral analysis is applied to the low-frequency IMFs to identify the periodic signals (Ray et al., 2008). Finally, the IMFs containing periodic signals are selected and combined. Meanwhile, the classic ~~least squares (~~LS~~)~~ is employed for comparison. ~~Generally, the function model includes annual, semi-annual, and the 1st to 6th draconitic-year periodic signals (Li et al., 2018). Specifically, the LS formulation is as follows:~~ Generally, the function model includes annual, semi-annual, the 1st to 6th draconitic-year periodic signals (Ray et al., 2008), offsets and afterslips. The afterslip term is typically expressed in the form of logarithmic or exponential functions (Hetland and Hager, 2006; Nishimura, 2014; Tobita, 2016), and in this paper, we adopt an exponential decay function model. Specifically, the functional model can be expressed as,

$$x(t) = a + bt + \sum_{i=1}^{8}(c_i \cdot \sin(2\pi \cdot f_i \cdot t) + d_i \cdot \cos(2\pi \cdot f_i \cdot t)) + \sum_j e_i \cdot H(t - t_j) + \sum_z g_z \cdot (1 - e^{-\frac{(t-t_z)}{\tau_z}}) + n(t)\ , \quad (4)$$

Where $t$ is the observation time, $a$ is the initial position constant, $b$ is the linear rend, $c_i$, $d_i$ is the coefficient of the periodic signal ($c_1$ and $d_1$ represent the annual periodic coefficients, while $c_2$ and $d_2$ represent the semi-annual periodic coefficients, others are draconitic-year periodic coefficients), ~~$f_i$ is the period frequency,~~ $f_i$ is the frequency, $e_i$ is the offset magnitude, $t_j$

is the moment of offset occurrence, $H$ is the Heaviside function, $g_z$ is the afterslip magnitude, $t_z$ is the seismic event occurrence time, $\tau_z$ is the relaxation time and $n(t)$ is the noise term.

Last but not the least, the assessment of the ~~extracted~~ signal reliability is crucial, which can be measured in different perspectives. Generally, it is measured by correlation coefficients (CC), root mean square error (RMSE), mean absolute error (MAE), power spectral density ~~(PSD)~~index ($\kappa$) and ~~signal noise ratio~~signal-to-noise (SNR) (Bos et al., 2008; Chen et al., 2020; Ran et al., 2022). Their specific calculation formulas are as follows,

$$CC = \frac{\sum_{i=1}^{N}(X_i-\bar{X})(Y_i-\bar{Y})}{\sqrt{\sum_{i=1}^{N}(X_i-\bar{X})^2\sum_{i=1}^{N}(Y_i-\bar{Y})^2}}, \tag{5}$$

$$RMSE = \sqrt{\frac{\sum_{i=1}^{N}(X_i-Y_i)^2}{N}}, \tag{6}$$

$$MAE = \frac{\sum_{i=1}^{N}|X_i-Y_i|}{N}, \tag{7}$$

$$P(f) = P_0\left(\frac{f}{f_0}\right)^{\kappa}, \tag{8}$$

$$SNR = 10 \cdot log_{10}\left(\frac{\sum_{i=1}^{N}{X_i}^2}{\sum_{i=1}^{N}(X_i-Y_i)^2}\right), \tag{9}$$

Where $X_i$ and $Y_i$ are the true signal and prediction signal at the i-th sampling point, respectively. $\bar{X}$ and $\bar{Y}$ are the means of the two signals. $N$ is the length of the signal. $P(f)$ is the power spectral density of the signal, $f$ is the frequency, $P_0$ and $f_0$ are constants representing the amplitude and reference frequency, and $\kappa$ is the power spectral density index obtained through linear fitting. However, in the practical analysis of stations, there is no true signal present. Therefore, $X_i$ and $Y_i$ represent the values at the ith sampling point for the post-processed vertical components (outliers removed, missing data filled and offset corrected) and the extracted periodic signal, respectively. $P(f)$ denotes the power spectral density of the residual signal $(X_i - Y_i)$. Due to the true signal known in the simulated experiments, the extracted signal was evaluated using the RMSE and MAE. For the real data analysis, the CC, RMSE, $\kappa$, and SNR were employed. Specifically, the higher ~~correlation coefficient~~ CC of the extracted periodic signal and the original time series, the more accurate extraction. A smaller RMSE indicates a more accurate extraction of the periodic signal. The ~~PSD index~~$\kappa$ of the residuals is used to evaluate the noise characteristics and indirectly reflects the accuracy of the extracted signal, of which the lower absolute values imply more accurate extraction. Similarly, the larger the SNR, the better the periodic model established.

## 3 Synthetic time series analysis

To test and validate the performance of the adaptive EEMD method, simulation experiments are carried out. In a simplified scenario, only annual and semi-annual periods are simulated as follows,

$$s(t) = a + bt + \sum_{i=1}^{2}(c_i \cdot \sin(2\pi \cdot f_i \cdot t) + d_i \cdot \cos(2\pi \cdot f_i \cdot t)), \quad \cancel{(5)}(10)$$

Specifically, the 5- year data $x(t)$ is simulated, which is generated with the parameters in Table 1. To be more realistic, not only white noise but also power-law noises are included ~~(Eq. (6))~~ (Eq. (11)). The magnitudes of white noise $p(t)$ and power-law noise $q(t)$ are 0.6 mm and 2 $\mathrm{mm}^{-0.6}$. That means the power-law spectral index here is -0.60.

**Table 1. The Simulated parameters in synthetic time series (mm).**

| $a$ | $b$ | $c_1$ | $d_1$ | $c_2$ | $d_2$ |
|---|---|---|---|---|---|
| 5 | 2 | 10 | 10 | 5 | 5 |

$$x(t) = s(t) + p(t) + q(t)\ , \qquad \text{~~(6)~~(11)}$$

Since missing data and offset are the general cases, these are mainly investigated in this section.

### 3.1 Impact of missing data on adaptive EEMD

GNSS provides critical daily position time series for geodetic and geophysical studies. However, due to unforeseeable factors such as receiver malfunctions, human errors, or deteriorating environmental conditions, the occurrence of missing data is inevitable (Bao et al., 2021). ~~The presence of missing data can significantly impact time series analysis. Therefore, selecting an appropriate approach is crucial when addressing the issue of missing data in GNSS position time series. To address it, the IEMD method is used in data filling, due to its dual advantage of efficient and accurate. However, this could be influenced by the percentage of missing data. Given the complex actual situations, missing data might appear randomly or consecutively.~~ The IEMD method described in Sect. 2 is used in data filling, due to its advantage of efficient and accurate. However, its performance could be influenced by the percentage of missing data. Since there are no true data at the missing epochs, it is impossible to evaluate the performance. Therefore, the missing data in the simulations are artificial deletion from the original data. In practice, data missing may occur randomly or consecutively (Shen et al., 2014). To be more realistic, randomly missing and consecutively missing cases are simulated through deleting data from original data. For the randomly missing~~ data~~, we removed 5%, 10%, 15% and 20% ~~of~~from the original ~~data ~~time series data.~~; for consecutively missing data,~~ While for the simulations of consecutive missing, we randomly deleted data for 15, 30, 45 and 60 consecutive days. Here, we present an example with a missing rate of 15% and a consecutive 30 days missing (Fig.2~~ Fig.5~~). We can see that data marked in red are filled by IEMD, which preserves the same variation of the original time series. The decomposition of the filled data using adaptive EEMD are shown in Fig. 3. From the IMFs, it is easy to identify the simulated annual (IMF6) and semi-annual (IMF5) signals. Figure 4 demonstrates the obtained periodic signal with the real periodic signal. As expected, the results indicate that with the increase in the percentage of missing data, the extracted periodic signal gradually deviates from the true values. In order to obtain more reliable statistical results, each simulation is carried out 300 times. The mean RMSEs and MAEs of each simulation are presented in Fig. 5. As depicted in the figure, it can be observed that with the increase of the missing data, both RMSE and MAE gradually increase, which indicates that the stability of the filling results is decreasing and may lead to larger errors. Especially when the random missing data rate reaches 15%, RMSE and MAE show the rapid increases, at 0.11 and 0.05, respectively, when consecutively missing data points is between 30 and 45, the increase of RMSE and MAE is more pronounced, at 0.32 and 0.06, respectively. Therefore, to ensure the accuracy and reliability of adaptive EEMD, the overall random missing rate should be less than 15%, and the consecutive missing epochs should be less than 30 days.

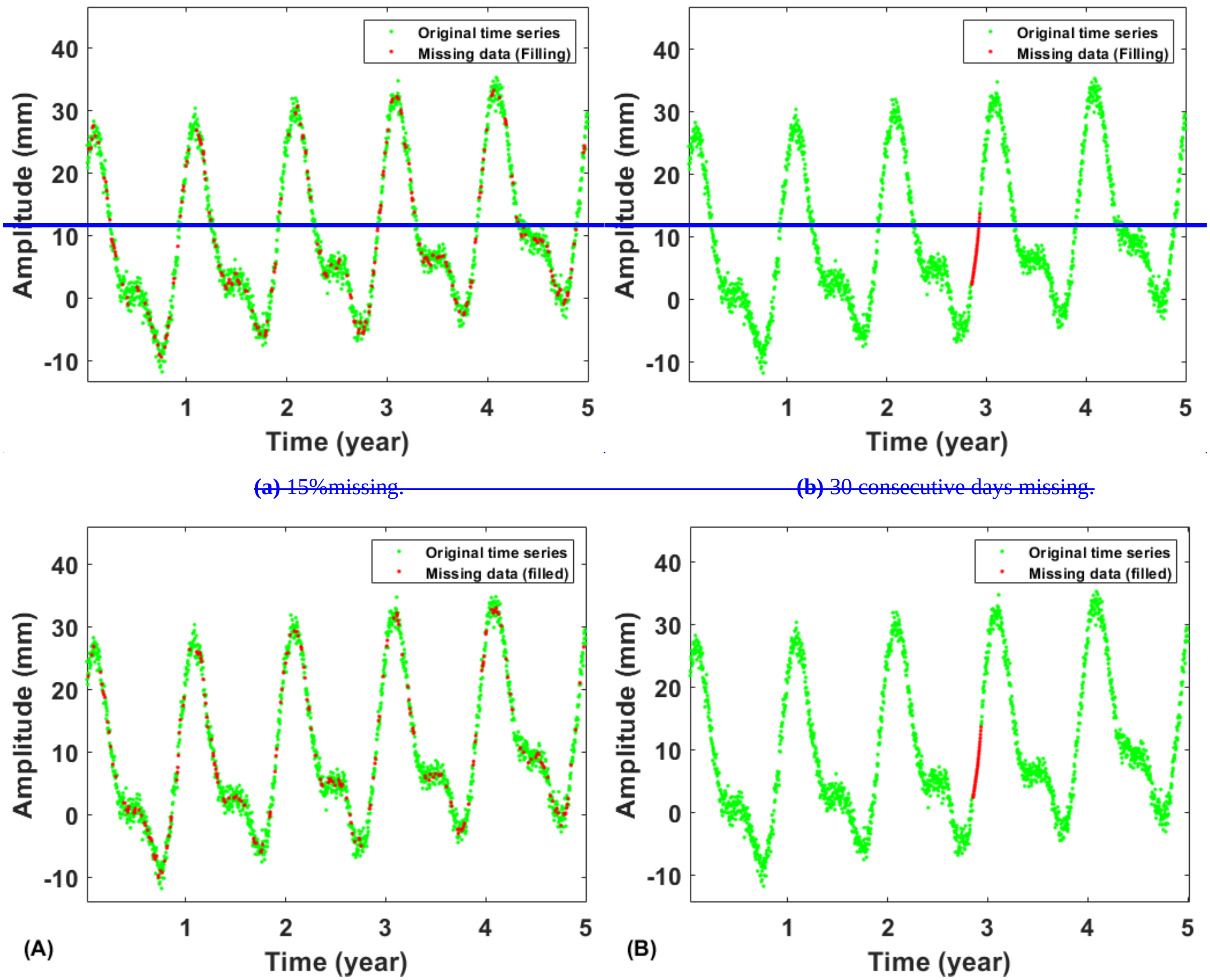


**Figure 2: Data filling of ~~(a)~~(A) random missing 15% and ~~(b)~~(B) consecutive missing 30 days.**

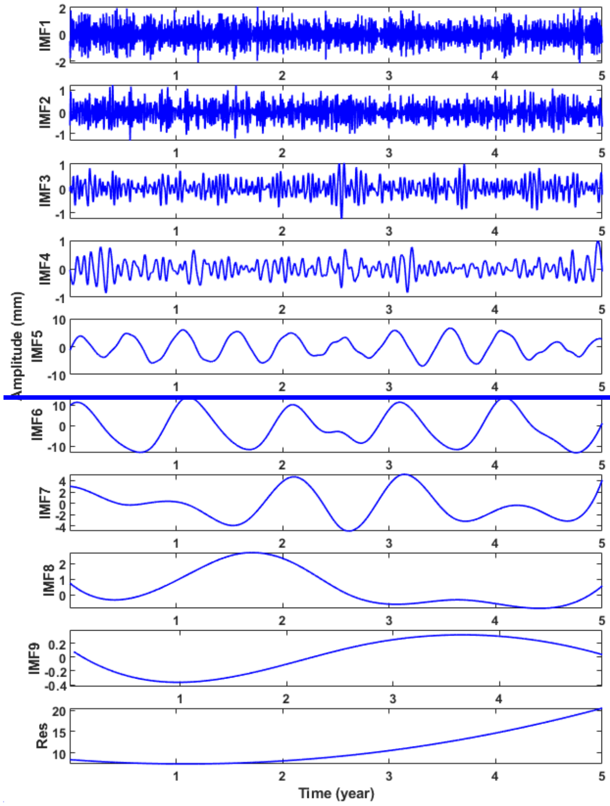


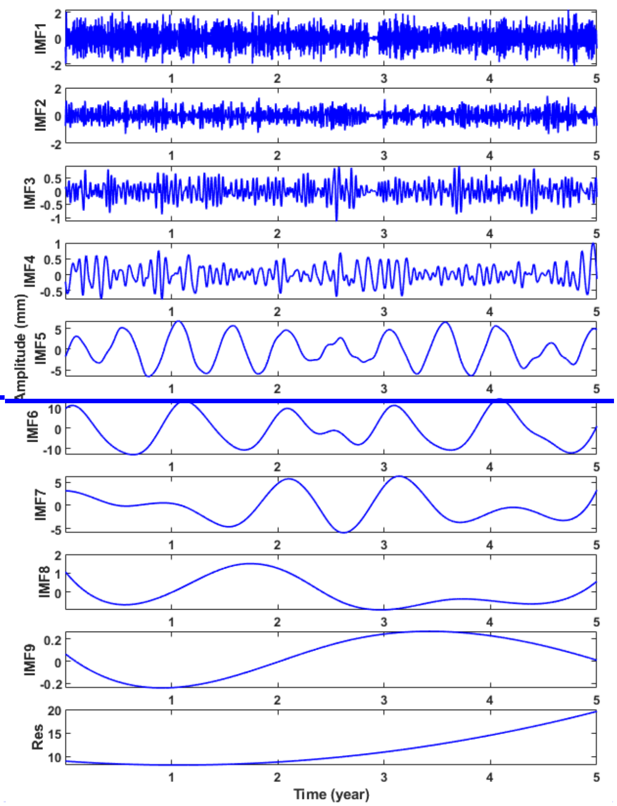


225

~~**(a)** 15%missing.~~ ~~**(b)** 30 consecutive days missing.~~

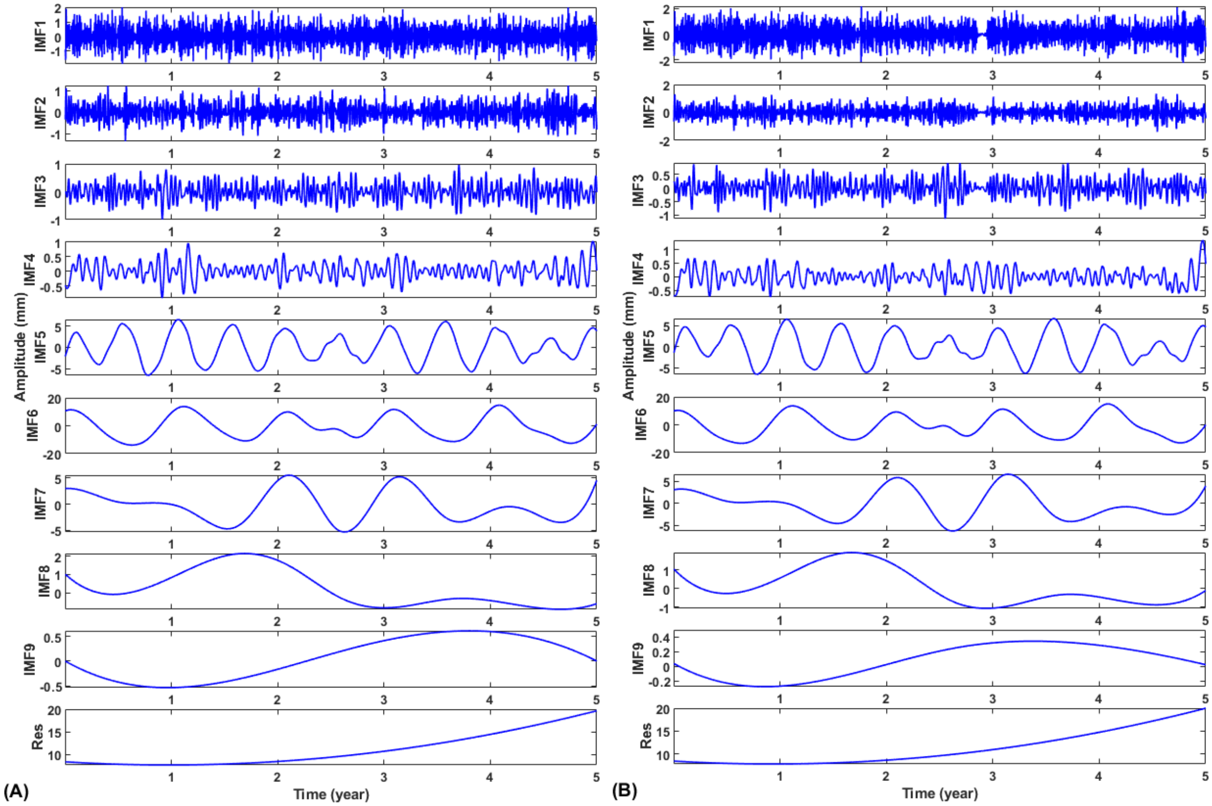


**Figure 3: Decomposition of filled series with adaptive EEMD ~~(a)~~(A) random missing 15% and ~~(b)~~(B) consecutive missing 30 days.**

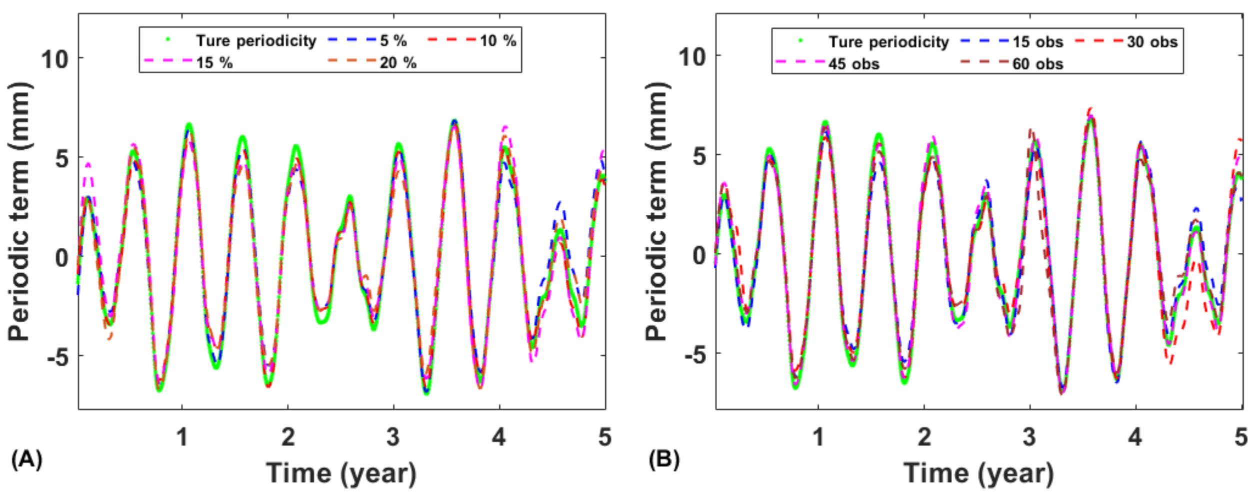


**Figure 4: The obtained periodic signal and the real periodic signal of (A) randomly missing and (B) consecutively missing.**

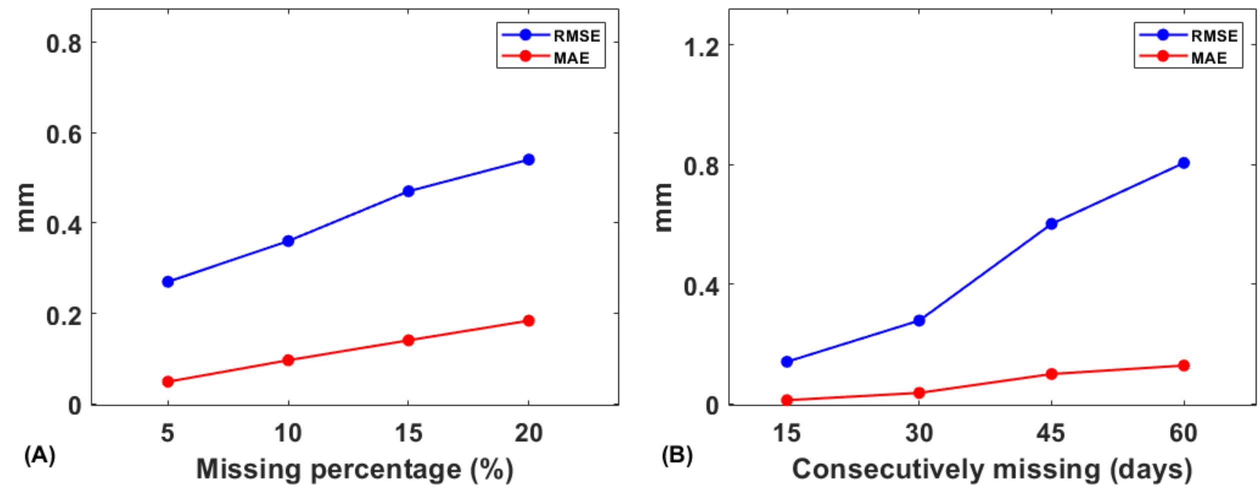


**Figure 5: RMSE and MAE of (A) randomly missing and (B) consecutively missing.**

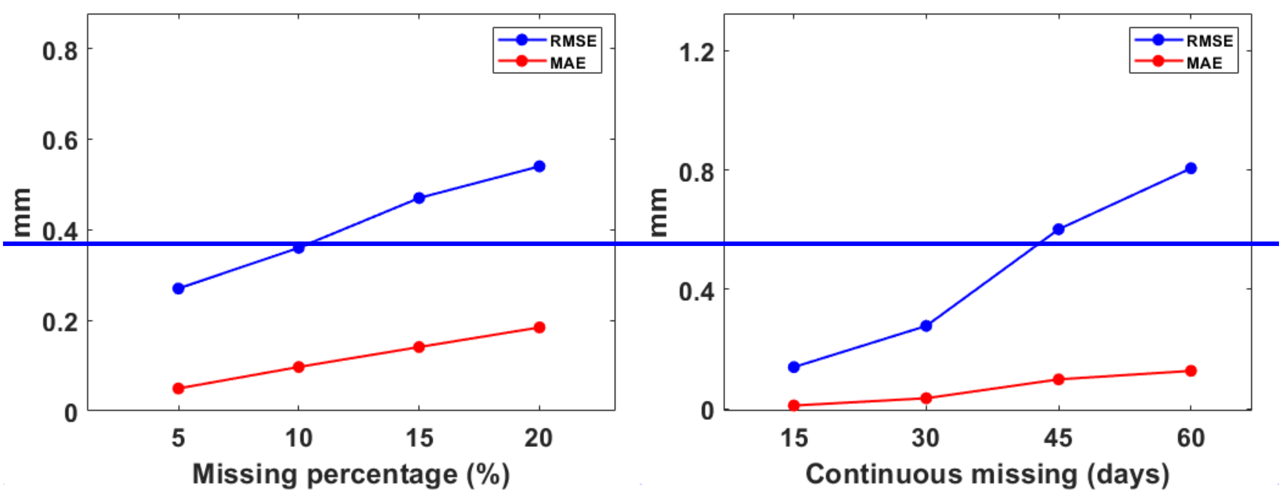


~~**(a)** randomly missing.~~ ~~**(b)** consecutively missing.~~

~~**Figure 4: RMSE and MAE of (a) randomly missing and (b) consecutively missing.**~~

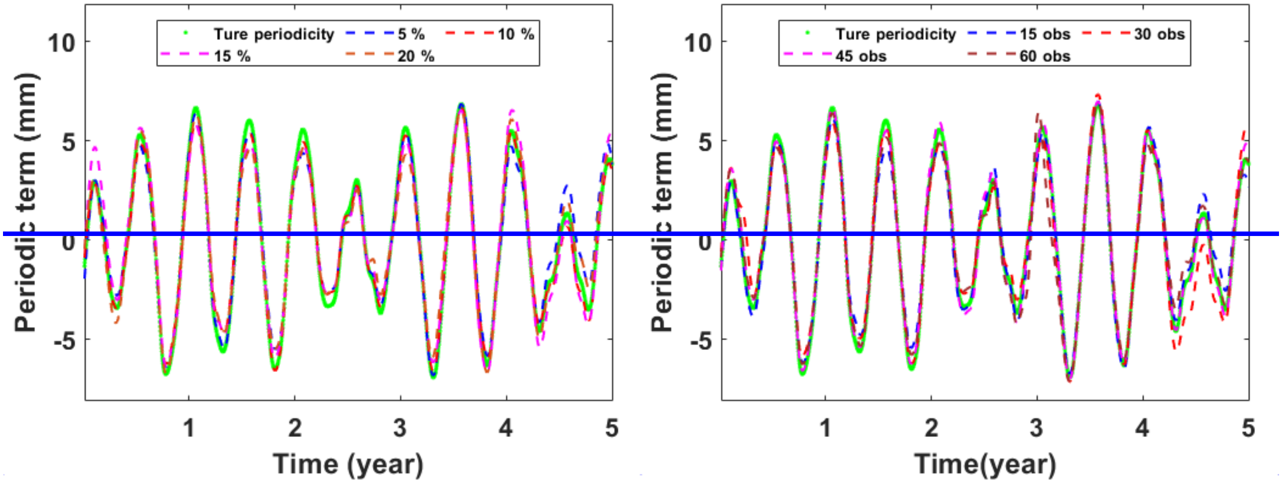


~~**(a)** randomly missing.~~ ~~**(b)** consecutively missing.~~

~~**Figure 5: The obtained periodic signal and the real periodic signal of (a) randomly missing and (b) consecutively missing.**~~

~~The results of filling in the missing data are shown in Fig. 2, which keeps the same variation of the original time series. The results of the adaptive EEMD are shown in Fig. 3. The decomposition components indicate that the simulated annual and semi-annual signals are clear. The mean RMSEs and MAEs of 300 simulations in different missing percentages are presented in Fig. 4. As depicted in the figure, it can be observed that with the increase of the missing data percentage, both RMSE and MAE gradually increase, which indicates that the stability of the filling results is decreasing and may lead to the error increased. Especially when consecutively missing data points is between 30 and 45, the increase of RMSE and MAE is more pronounced. Figure 5 demonstrates the obtained periodic signal with the real periodic signal. As expected, the results indicate that with the increase in the percentage of missing data, the extracted periodic signal gradually deviates from the true values.~~

~~Therefore, to ensure the accuracy and reliability of adaptive EEMD, the overall random missing rate should be less than 15%, and the consecutive missing epochs should be less than 30.~~

### 3.2 Impact of offset on adaptive EEMD

The offsets caused by satellite orbit changes, receiver hardware or software problems, data processing algorithm improvements, and other unknown factors are common in GNSS time series ~~(Defraigne et al., 2021)~~ (Gazeaux et al., 2013). For the known offsets, in data preprocessing, the magnitudes of offsets are estimated according to the epochs of earthquake or instrument replacement, then the known offsets are corrected. However, for the unknown factors, it is difficult to detect the offset time due to the outliers and noises included. While the percentage due to unknown factors can be up to 20%, its influence cannot be ignored (Griffiths et al., 2016). Therefore, it is urgent to identify and correct the offset. Although there are many methods to detect the offset ~~(Feng et al., 2013; Wang et al., 2019)~~ (Wang and Herring, 2019; Tehranchi et al., 2020), neither is 100% effective. To verify the offsets correction essential or not, tests (with and without offset correction) are carried out. Traditionally, manual visual inspection is combined with the STARS method for offset detection, and the LS method is used for offset correction (Rodionov, 2004; Cai, 2020). Since the number and magnitude are the two factors of offsets, these are variables in the simulations. Specifically, the offset number ranges from 2 to 8, with an interval of 2. The simulated offset magnitudes are 0.5σ, 1.0σ, 1.5σ, 2.0σ and 2.5σ mm (Su et al., 2023), with standard deviation (σ) of the simulated time series (σ=12.70 mm). Also, the simulations are repeated 300 times. Since our focus is the extraction of periodic signals, the effect of simulated offsets on the periodic signals is analyzed. Accordingly, the RMSE and MAE between the periodic signals obtained using the adaptive EEMD method with and without offset correction and the real periodic signal are ~~compared. They are~~ shown in Fig. 6.

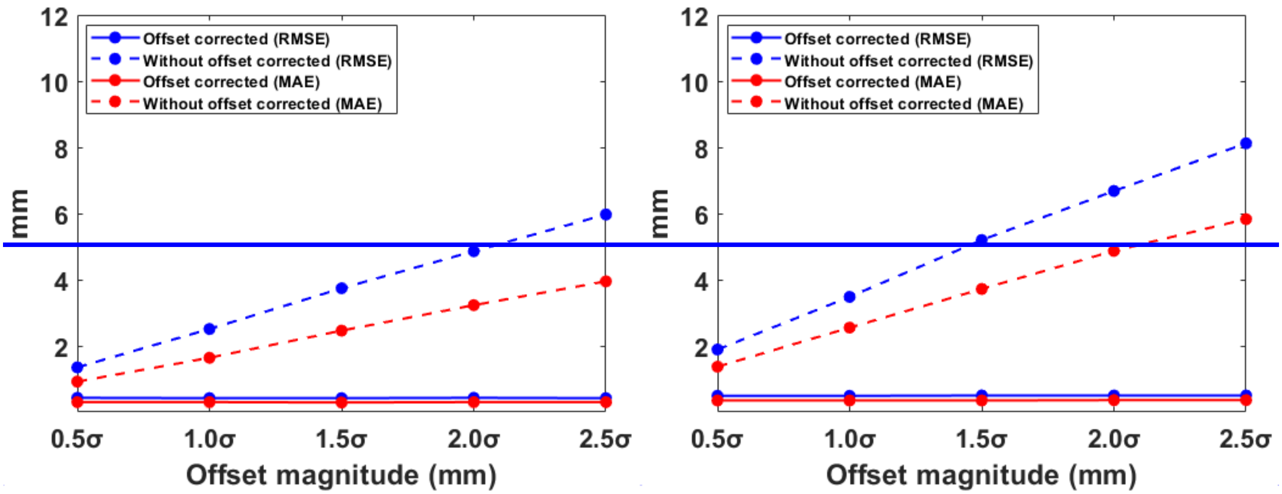


~~(a) 2 offsets.~~ ~~(b) 4 offsets.~~

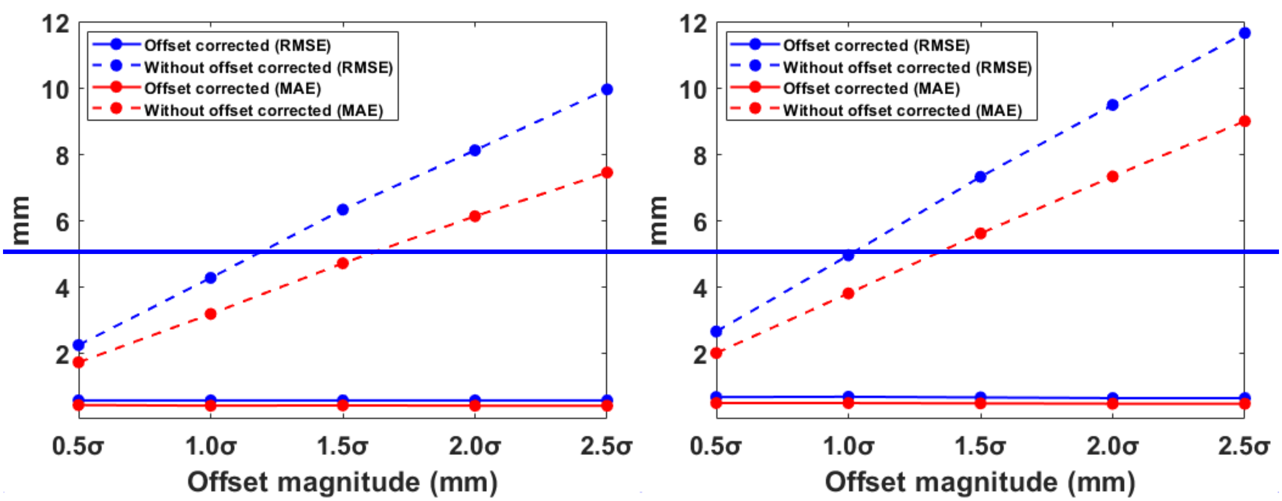


~~(c) 6 offsets.~~ ~~(d) 8 offsets.~~

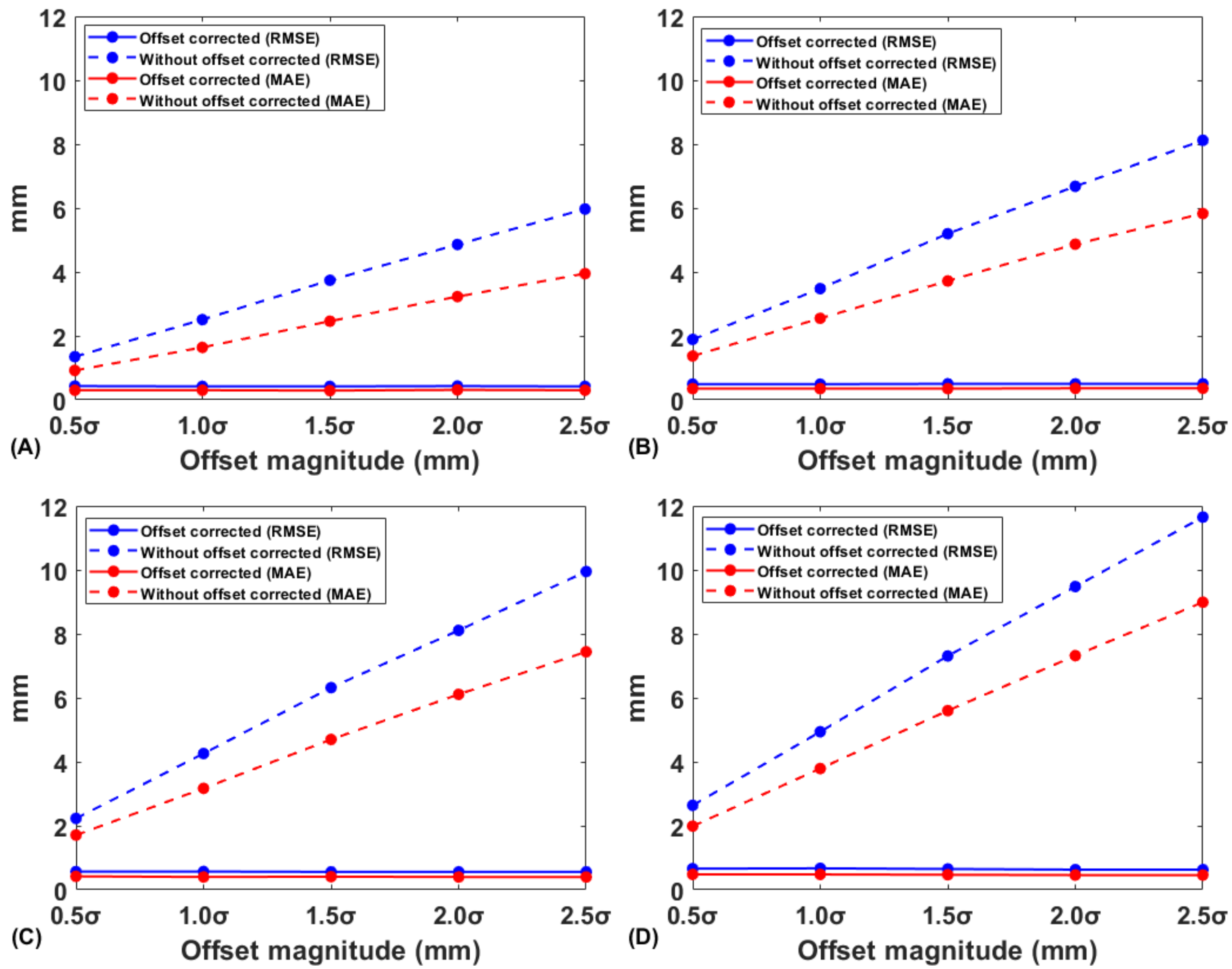


**Figure 6: Periodic signal RMSE and MAE with and without offset correction of different number and magnitude offsets ~~(a)~~(A) 2 offsets, ~~(b)~~(B) 4 offsets, ~~(c)~~(C) 6 offsets and ~~(d)~~(D) 8 offsets.**

It is found that when no correction beforehand, RMSE and MAE rapidly increase as the magnitude and number of offsets increase. With the offset corrected, both RMSE and MAE reveal substantial decrease. This ~~reveals~~indicates that in adaptive EEMD application, the presence of offsets significantly ~~reduce~~ leads to the reduction of the accuracy of periodic signal extraction. ~~From the improvement ratio in Table 2,~~ Further the improvement ratio of offset correction to without correction is shown in Table 2. ~~we~~We can see that even when the offset magnitude is 0.5σ and offset number is 2, the ratios for RMSE and MAE are 68.15% and 67.39%, respectively. Meanwhile, as offset number increases, the improvement ratios for RMSE and MAE gradually rise. This indicates the necessity of offset correction even in condition of ~~very~~ small ~~offset~~ magnitude. However, these findings are based on the all the offsets detected are accurate, although in reality, it is hard to realize. Thus, it is recommended to perform offset correction for the adaptive EEMD application in the GNSS coordinate time series analysis.

**Table2. The improvement ratios of RMSE and MAE with an offset magnitude of 0.5σ.**

| Number of offsets | Improvement ratio (%) | |
|---|---|---|
| | RMSE | MAE |
| 2 | 68.15 | 67.39 |
| 4 | 74.07 | 74.45 |
| 6 | 74.89 | 75.44 |
| 8 | 75.00 | 75.88 |

## 4 Results and analysis

### 4.1 Data sources

Thirteen GNSS stations located in the Australian region are selected for the study, and their locations are shown in Fig. 7. The vertical components for these selected stations can be downloaded from the Sonel website (https://www.sonel.org/spip.php?page=cgps&lang=en, accessed in May 2023) ~~(Łyszkowicz and Bernatowicz, 2019)~~. Table 3 provides essential station information, including longitude and latitude coordinates, the time span, the raw missing rate (%) and the missing rate after gross error elimination (%), among which the longest time span is MAC1 station and the shortest one is BRO1 station. Additionally, the XMIS station exhibits the highest missing rate after outlier removal, which reaches 13.60%. The known offset epochs and magnitudes available from the ~~Sonel~~ SONEL website, as well as offset occurred in 2011.6123 at NORF station ~~determined~~ detected with STARS method, along with its magnitude estimated by LS, are shown in Table 4.

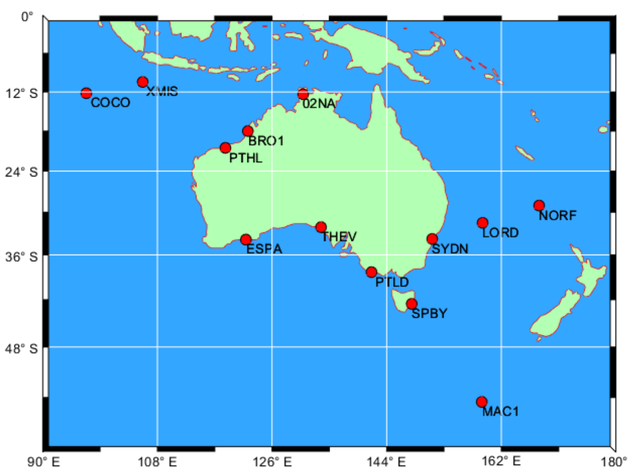


**Figure 7: Location of the selected 13 GNSS stations in Australia.**

**Table 3. GNSS stations information used in this study.**

| Site | Longitude (°) | Latitude (°) | Span (year) | Length (year) | Raw missing rate (%) | Missing rate after gross error elimination (%) |
|---|---|---|---|---|---|---|

| | | | | | | |
|---|---|---|---|---|---|---|
| THEV | 133.6968 | -32.1286 | 2014.8726-2020.1189 | 5.25 | 3.44 | 4.27 |
| XMIS | 105.6884 | -10.4499 | 2005.4890-2020.9303 | 15.44 | 13.15 | 13.60 |
| SYDN | 151.1503 | -33.7808 | 2004.3429-2020.9932 | 16.65 | 5.16 | 5.54 |
| SPBY | 147.9308 | -42.5464 | 2008.7336-2013.9959 | 5.26 | 4.99 | 6.03 |
| PTLD | 141.6134 | -38.3444 | 2009.7712-2020.9932 | 11.22 | 8.07 | 8.48 |
| PTHL | 118.6788 | -20.5397 | 2016.8624-2021.9849 | 5.12 | 1.12 | 1.81 |
| NORF | 167.9388 | -29.0433 | 2008.4768-2020.9959 | 12.52 | 6.18 | 6.31 |
| MAC1 | 158.9358 | -54.4995 | 1996.9850-2013.9959 | 17.01 | 8.30 | 8.98 |
| LORD | 159.0611 | -31.5198 | 2009.4836-2020.9686 | 11.48 | 8.05 | 8.69 |
| ESPA | 121.8943 | -33.8743 | 2008.4495-2020.9418 | 12.49 | 6.16 | 6.61 |
| COCO | 96.8339 | -12.1883 | 1997.7521-2013.9959 | 16.24 | 7.02 | 8.96 |
| BRO1 | 122.2090 | -18.0039 | 2015.8808-2020.9658 | 5.09 | 6.99 | 8.06 |
| 02NA | 130.8817 | -12.3559 | 2008.7255-2014.0890 | 5.36 | 7.44 | 7.90 |

**Table 4. Offsets of the investigated 13 GNSS stations.**

| Site | Offset epoch (year) | Offset magnitude (mm) |
|---|---|---|
| THEV | \ | \ |
| XMIS | 2006.5411\2007.6973\2012.2801\2014.4836 | 1.9\-2.5\0.7\-0.7 |
| SYDN | \ | \ |
| SPBY | \ | \ |
| PTLD | 2012.1052\2012.3347\2012.9331\2017.4836\2018.3192 | 0.3\0.9\0.5\8.1\-7.7 |
| PTHL | \ | |
| NORF | 2011.6123\2016.7582 | 3.2\1.8 |
| MAC1 | \ | \ |
| LORD | \ | \ |
| ESPA | 2016.1544 | -4.8 |
| COCO | \ | \ |
| BRO1 | \ | \ |
| 02NA | \ | \ |

### 4.2 Data processing and analysis

In this section, we carry out a comparative analysis of the periodic signal in the vertical component of the 13 selected GNSS stations derived by adaptive EEMD method and the LS method. Figure 8 presents the post-processed vertical components (outliers removed, missing data filled and offset corrected) and the extracted signal. ~~It is evident that the adaptive EEMD method provides a superior fit to the original time series due to its time-varying characteristics.~~ It is apparent that the signal extracted is significantly different, from which adaptive EEMD method shows its advantage in time-varying signal extraction. For example, the signal of XMIS and ESPA demonstrate apparent peak signal in 2016 and 2015. To further evaluate its performance, ~~Figure 9 displays comprehensive assessment indicators.~~ comprehensive assessment indicators are displayed in Fig. 9. It is observed that the higher CC (Fig.9A), the lower RMSE (Fig.9B), the lower absolute of $\kappa$ (Fig.9C), the higher SNR (Fig.9D) of the adaptive EEMD, which shows its outstanding advantage over LS.

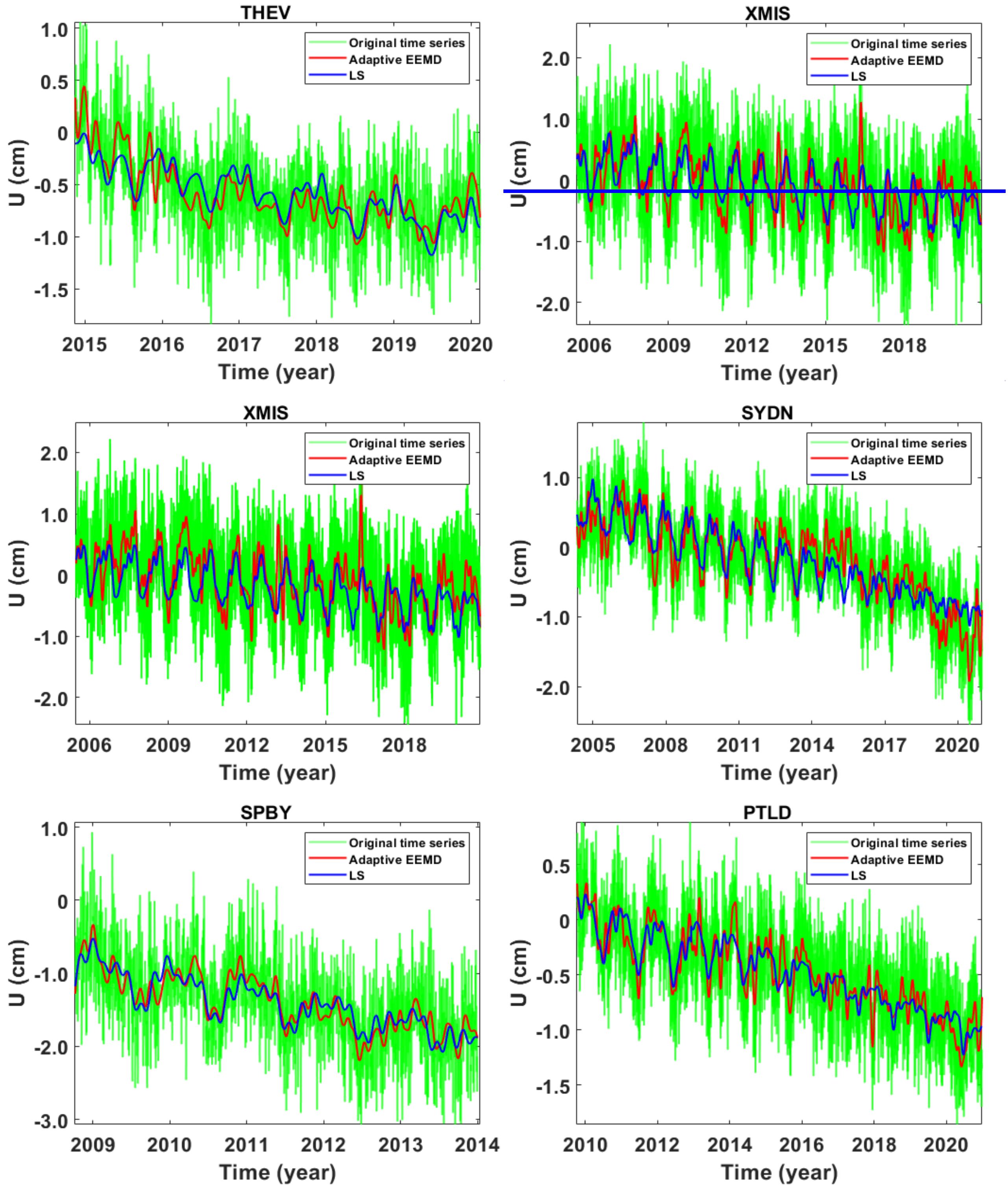
THEV
XMIS
XMIS
SYDN
SPBY
PTLD
Original time series
Adaptive EEMD
LS
U (cm)
Time (year)

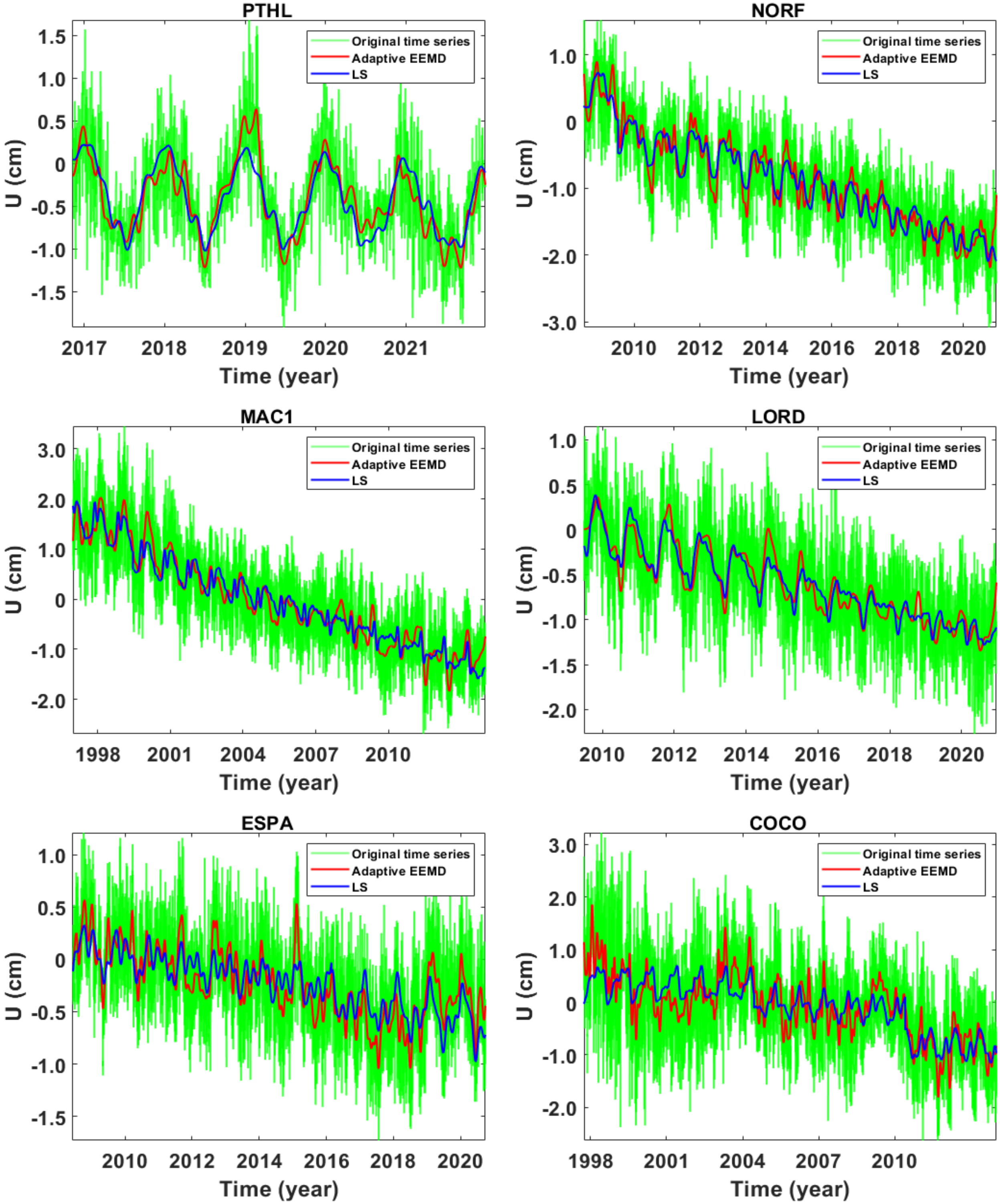
PTHL
Original time series
Adaptive EEMD
LS
U (cm)
1.5
1.0
0.5
0
-0.5
-1.0
-1.5
2017
2018
2019
2020
2021
Time (year)
NORF
Original time series
Adaptive EEMD
LS
U (cm)
1.0
0
-1.0
-2.0
-3.0
2010
2012
2014
2016
2018
2020
Time (year)
MAC1
Original time series
Adaptive EEMD
LS
U (cm)
3.0
2.0
1.0
0
-1.0
-2.0
1998
2001
2004
2007
2010
Time (year)
LORD
Original time series
Adaptive EEMD
LS
U (cm)
1.0
0.5
0
-0.5
-1.0
-1.5
-2.0
2010
2012
2014
2016
2018
2020
Time (year)
ESPA
Original time series
Adaptive EEMD
LS
U (cm)
1.0
0.5
0
-0.5
-1.0
-1.5
2010
2012
2014
2016
2018
2020
Time (year)
COCO
Original time series
Adaptive EEMD
LS
U (cm)
3.0
2.0
1.0
0
-1.0
-2.0
1998
2001
2004
2007
2010
Time (year)

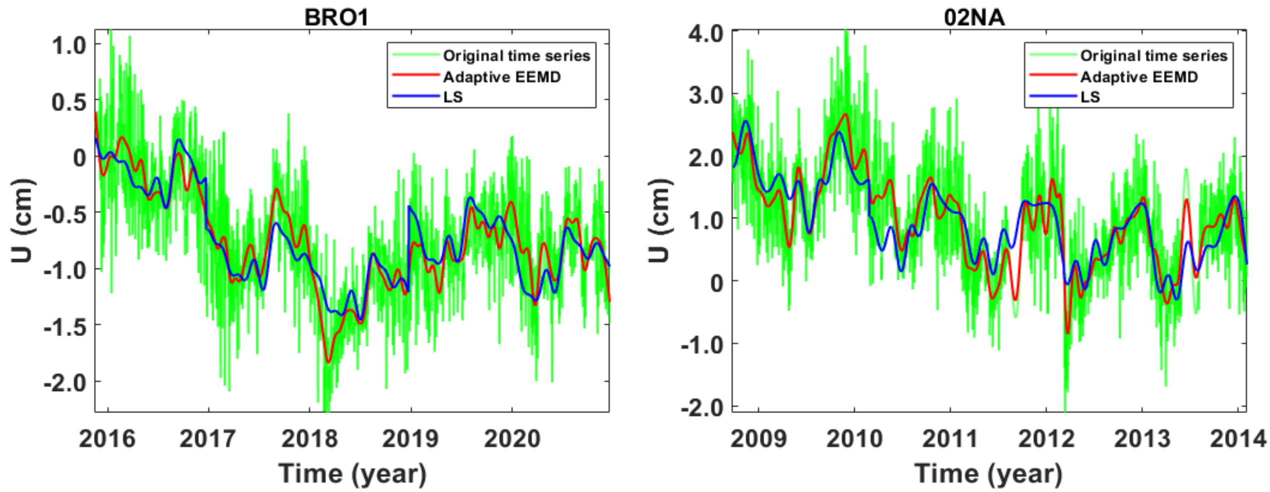


**Figure 8: Signals derived by adaptive EEMD and LS of the vertical components at 13 stations.**

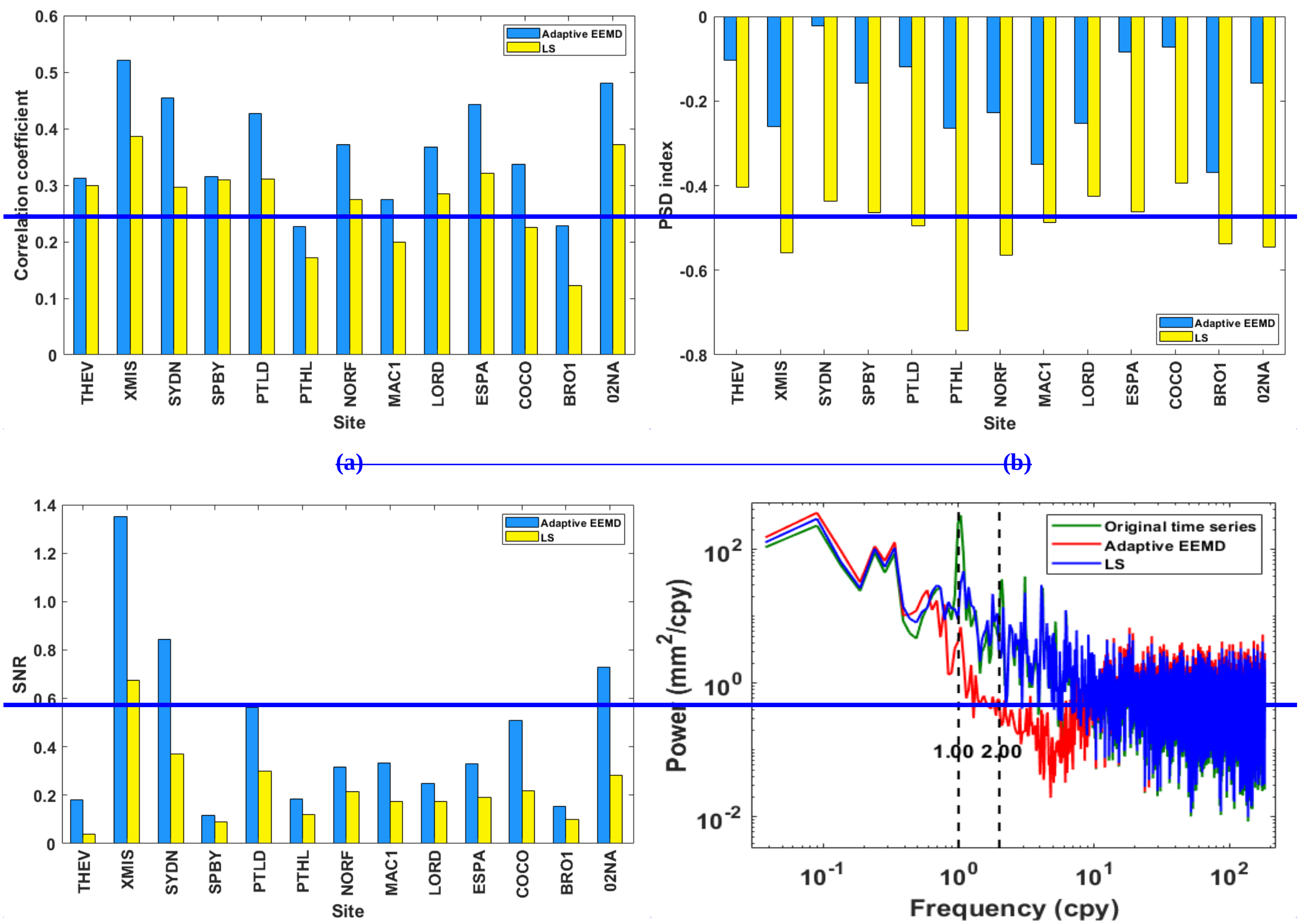


(a) (b)

(c) (d)

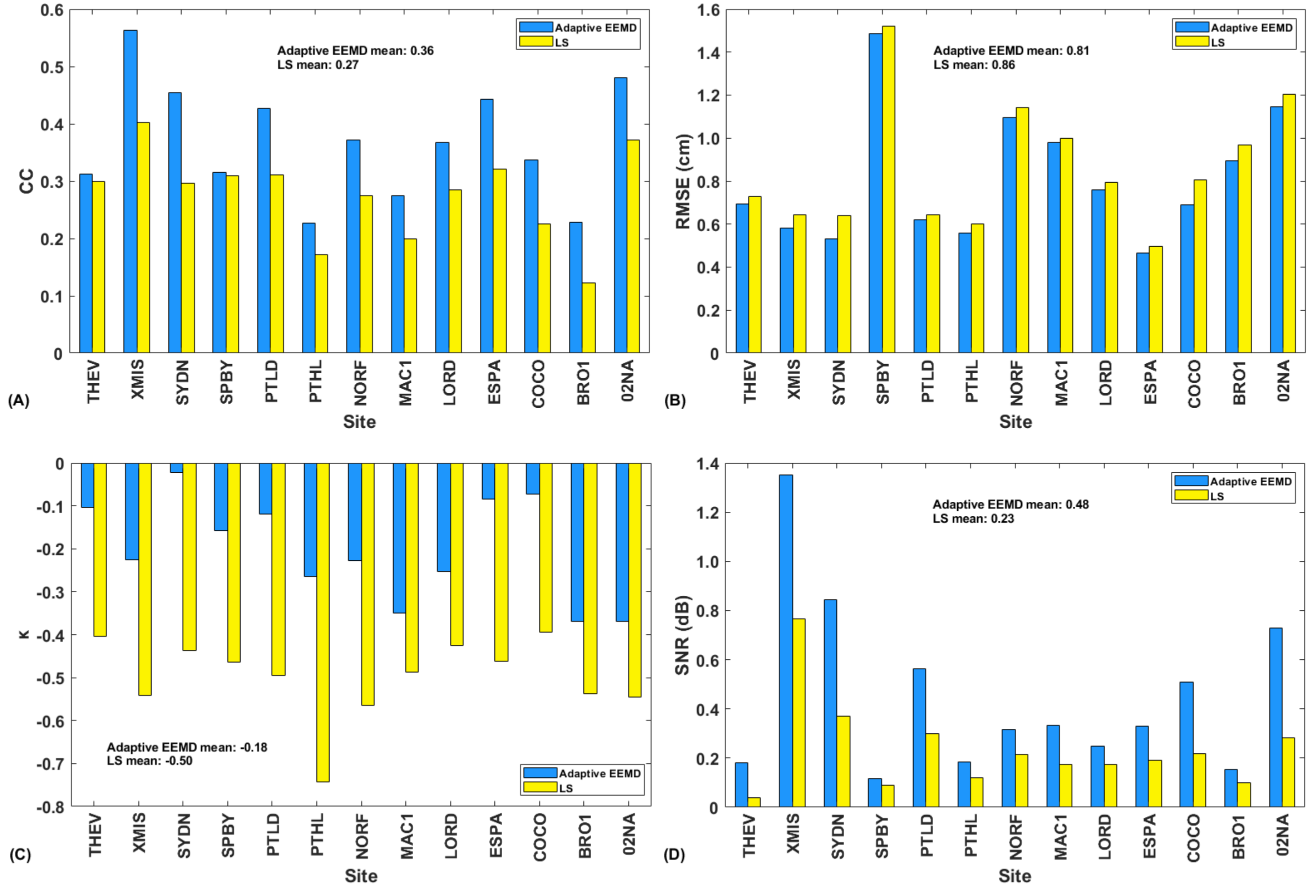


**Figure 9: Reliability indicators for periodic model assessing: ~~(a) Correlation coefficient, (b) PSD index, (c)SNR and (d) Stacked comparison of power spectrum analysis.~~(A) CC, (B) RMSE, (C) *κ* and (D) SNR.**

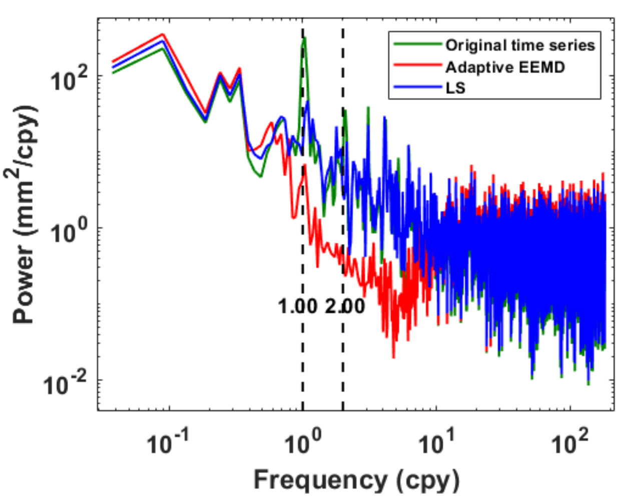


**Figure 10: Stacked comparison of power spectrum analysis.**

~~It is observed that the correlation coefficient of the adaptive EEMD method is higher than that of the LS method, while the absolute value of the PSD index of the adaptive EEMD method is lower, which suggests that it can effectively explain the variations of the original time series. And the SNR of the adaptive EEMD methods are all higher than the LS method, which further verifies their excellent performance in capturing signals.~~ In addition, power spectral stacking analysis is performed on residual ~~signals~~ obtained from 13 stations. ~~after using two methods for periodic signal extraction, Observations reveal that the periodic signals extracted by the adaptive EEMD method are 'cleaner' and better.~~ From Fig.10 we can see that residuals derived by adaptive EEMD has the lower power of frequency band that periodic signals existed than LS. However, it is also noted that the residual signal using the adaptive EEMD method still shows an annual peak ~~in Fig. 9(d)~~. To confirm the significance of this signal within the residual signals, power spectral significance test is conducted (Horne et al., 1986; Press et al., 2010), as shown in Fig. ~~10~~11. The false alarm probability, which is used to estimate the significance of peaks in the power spectrum, indicating the probability of being a result of true signals as opposed to random noise distribution. Generally, lower values (<0.01) indicate higher probability. The results indicate that 1.00 cpy signal is not significant in the residuals. In contrast, the residual signal using the LS method still shows significant presence of the 1.00 cpy signal. This further highlights the superiority of the adaptive EEMD method in extracting periodic signals.

Moreover, the length of time series in EEMD application is an important factor to consider, which is essential to investigate the impact on periodic signals extracting. Thus, the aforementioned 13 stations are categorized into two groups based on data length: stations with time series exceeding 10 years (mean time series length of 14.13 years) and stations with time series shorter than 10 years (mean time series length of 5.21 years). Also, significance tests are conducted on stacked residual signals for these two groups of stations. As illustrated in Fig. ~~11-12~~12-13, the results demonstrate that the longer the time series, the better the performance of both methods in extracting periodic signals. Furthermore, the adaptive EEMD method outperforms in both scenarios, no matter for data longer or shorter than 10 years.

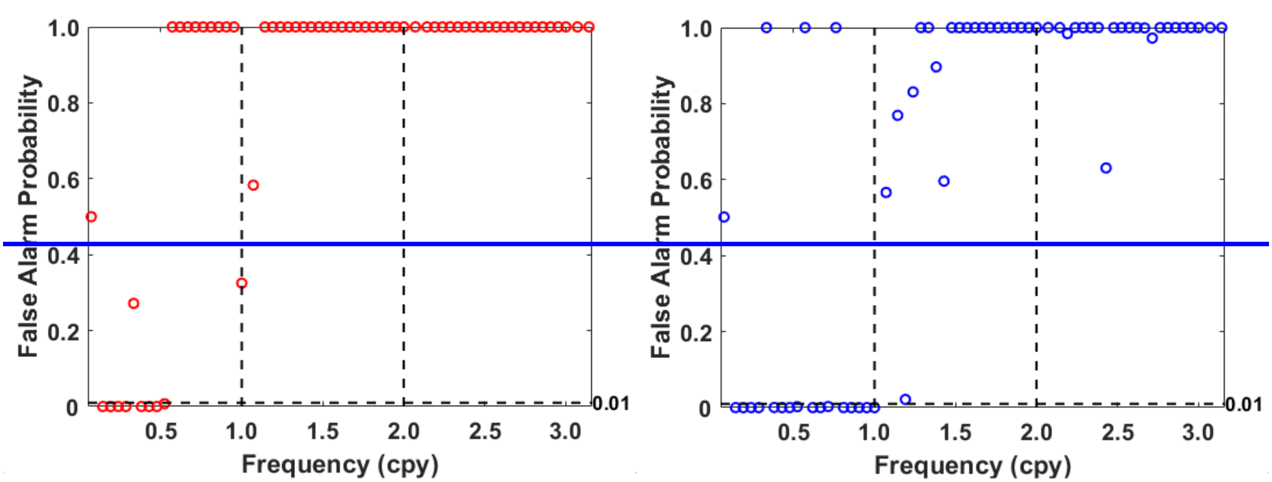


~~(a) Adaptive EEMD.~~ ~~(b) LS.~~

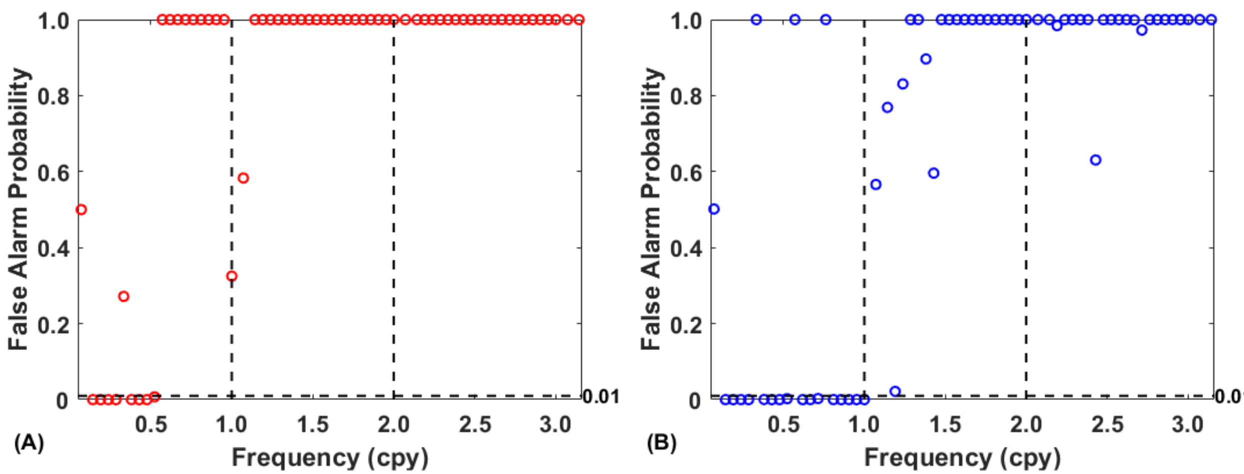


**Figure ~~10~~11: Significance test of residual signal derived from adaptive ~~(a)~~(A) EEMD and ~~(b)~~(B) LS.**

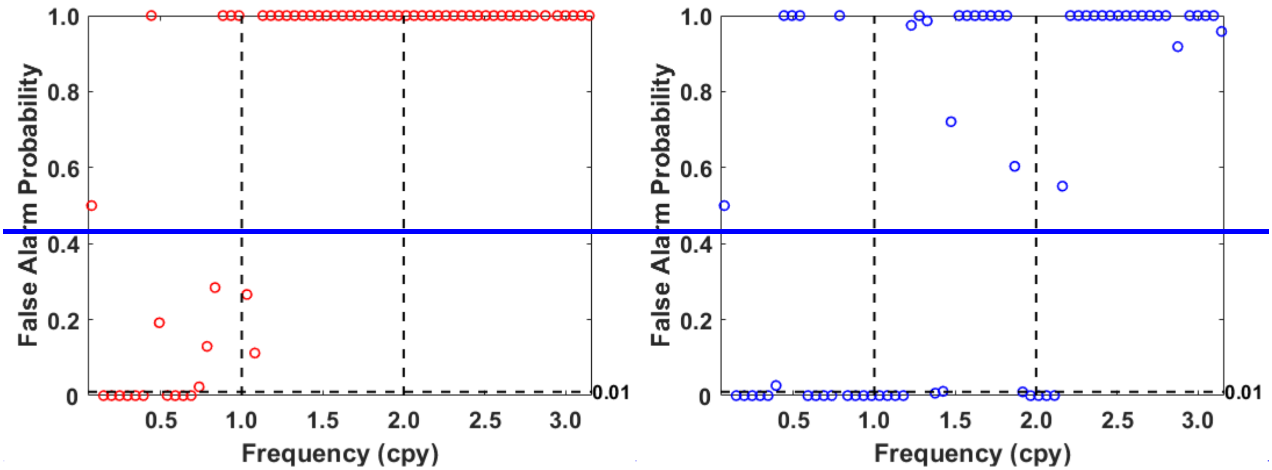


~~(a) Adaptive EEMD.~~ ~~(b) LS.~~

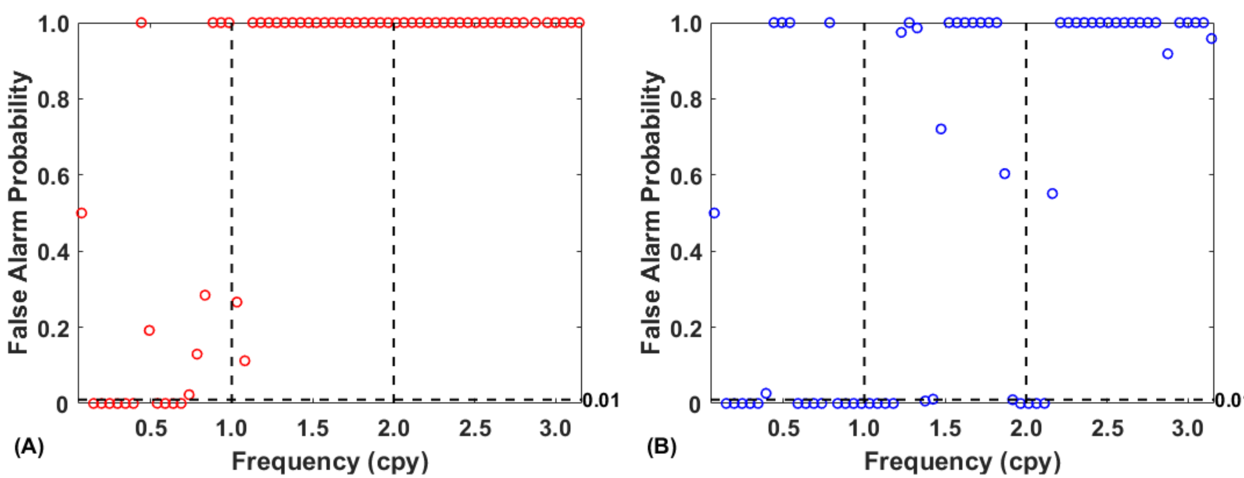

**Figure ~~11~~12: Significance test of residual signal derived from ~~(a)~~(A) adaptive EEMD and ~~(b)~~(B) LS for stations with data less than 10 years.**

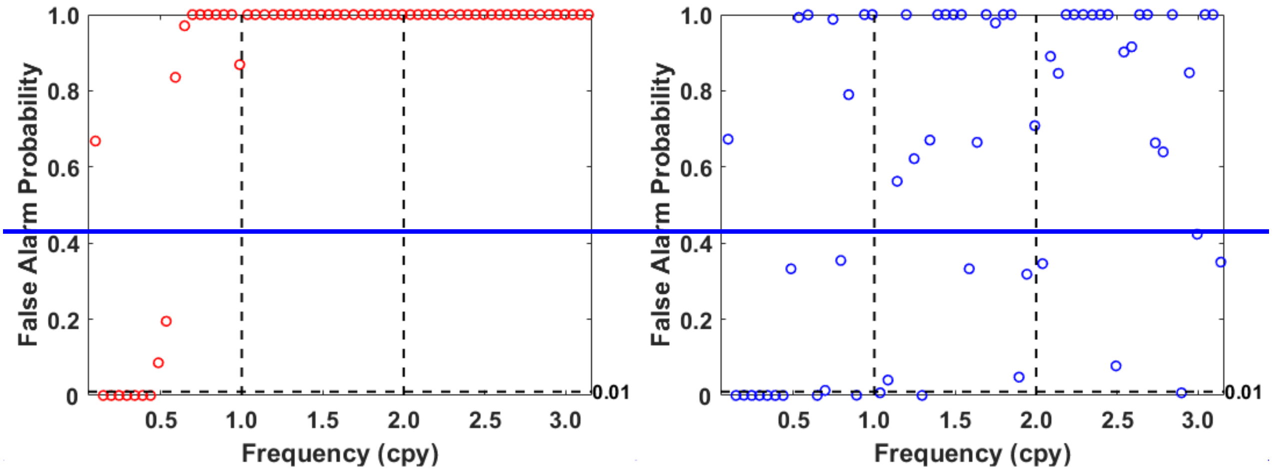


~~**(a)** Adaptive EEMD.~~ ~~**(b)** LS.~~

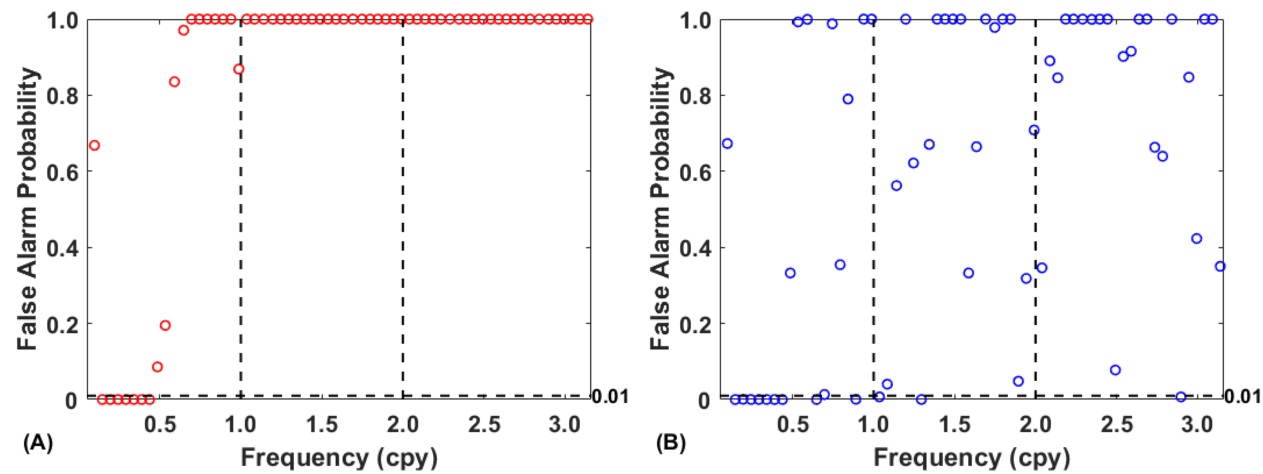


**Figure ~~12~~13: Significance test of residual signal derived from ~~(a)~~(A) adaptive EEMD and ~~(b)~~(B) LS for stations with data more than 10 years.**

### 4.3 Discussion

Figure ~~13~~14 displays all the periodic signals of the 13 stations in the vertical direction. It is evident that all the ~~13~~ stations exhibit significant periodic patterns, but with varying amplitudes. This may be significantly influenced by ~~extreme~~ geophysical phenomenon (Abraha et al., 2017). It is noteworthy that an anomalous peak is observed in the periodic signal of the XMIS station on 25 May 2016 (approximately 2016.35 years), characterized by an approximately twice larger amplitude of than its mean amplitude (which is approximately 0.5 cm). Similar phenomena are also observed at the ESPA station on 10 February 2015 (approximately 2015.11 years). To find a rational explanation, detailed analysis is conducted and utilized hydrological loading data from the EOST Loading Service (http://loading.u-strasbg.fr/listdata.php?dirn=dicf, accessed in July 2023)~~ (He et al., 2022)~~, which possesses a spatial resolution of 0.5° × 0.5° and a time resolution of 3 hours. Additionally, the daily rainfall time series provided by the Australian Bureau of Meteorology (http://www.bom.gov.au/climate/, accessed in July 2023) is adopted~~ (Pan et al., 2022)~~. Rainfall anomalies are defined as the difference between the daily rainfall and its mean value. The accumulated rainfall anomalies are obtained by summing the daily anomalies with the preceding days' anomalies (Singh et al., 2021). All the possible factors of the two example stations are demonstrated in Fig. ~~14~~15.

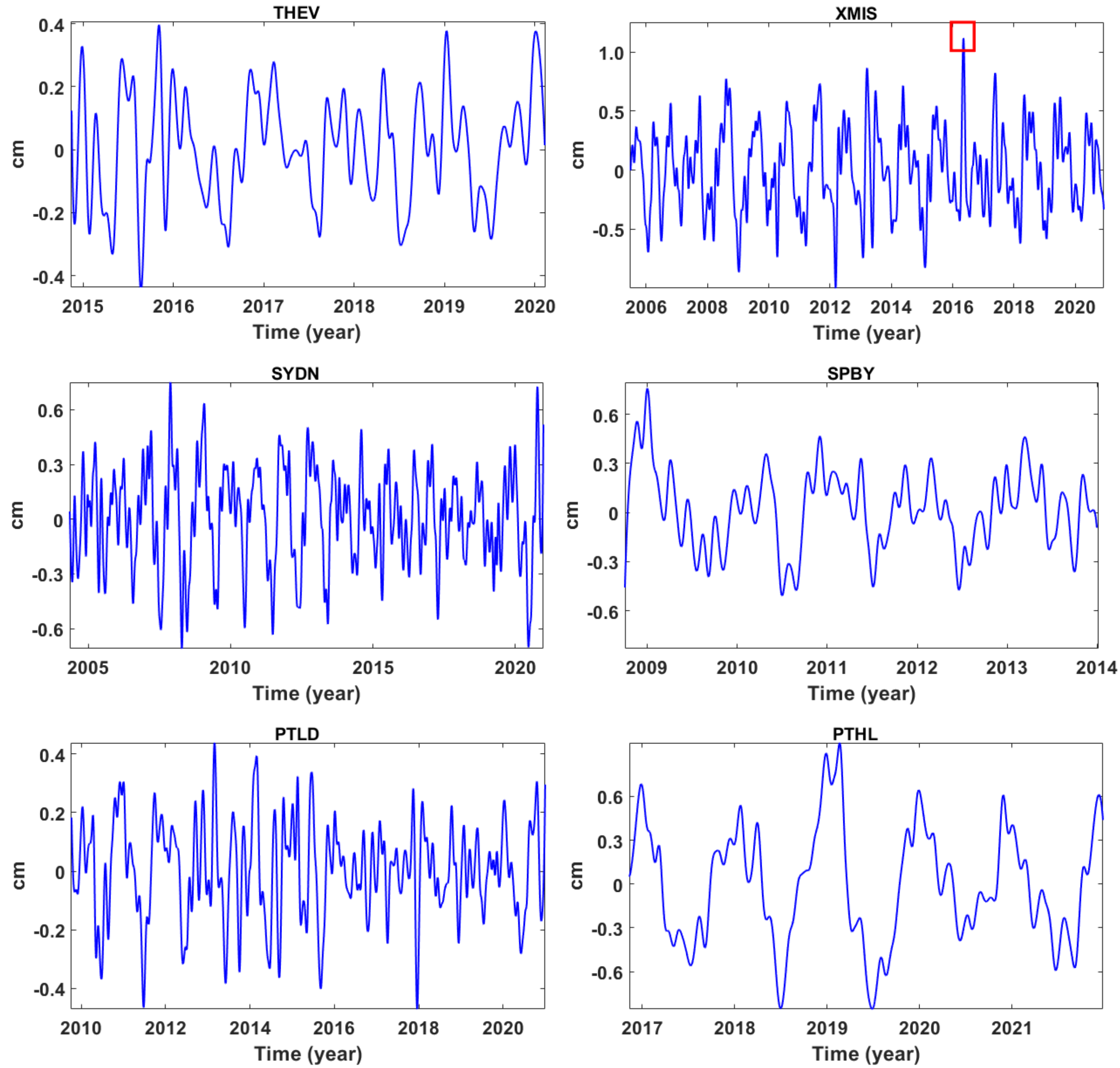

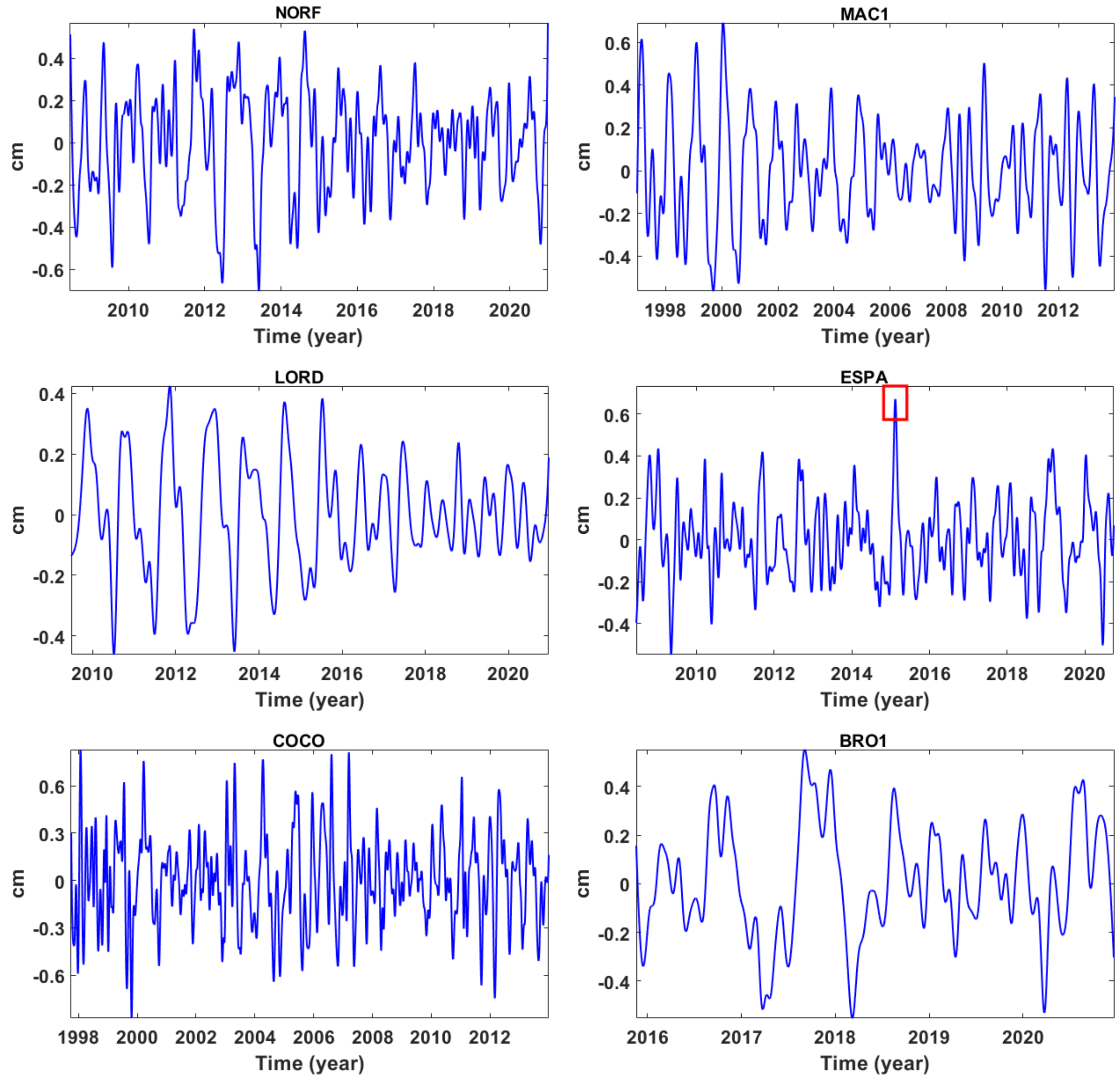
NORF
MAC1
LORD
ESPA
COCO
BRO1
cm
Time (year)

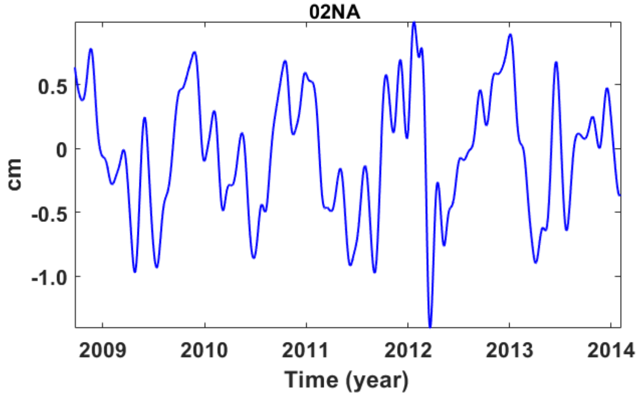


**Figure ~~13~~14: Periodic signals derived by adaptive EEMD of vertical components at 13 stations.**

We can see that the extremely low rainfall in the second half of 2015 led to the minimum accumulated rainfall anomaly at XMIS station on 7 May 2016. The increasing hydrological loading responded to the low rainfall but with a time lag reaching its maximum. According to the reports from the Australian Bureau of Meteorology indicated the presence of a strong El Niño phenomenon in 2016 (Kennedy et al., 2017) caused the spread of moist water vapor across the Australian continent. The hydrological loading decreased, which was affected by the rainfall directly. Meanwhile, the hydrological loading shows the visible annual features. The ~~high correlation coefficient~~ CC of 0.50 between hydrological loading data (detrended) and periodic signals for the year 2016, indicates that hydrological loading is one of the primary factors contributing to periodic changes. In addition, the ESPA station also exhibits a similar phenomenon around February 2015, with extremely low rainfall during the first three months of the year. This leads to a gradual decrease in accumulated rainfall anomalies, reaching its minimum on 29 March 2015. Hydrological loading during the same period reaches its current peak. The ~~correlation coefficient~~ CC between hydrological loading data (detrended) and the 2015 periodic signal is 0.57. This further emphasizes the significance of hydrological loading variations in relation to periodic changes. In summary, the primary characteristics of periodic variations are induced by hydrological loading, and other factors may also affect the periodic signals to some extent, which provides a direction for future research to explore in depth.

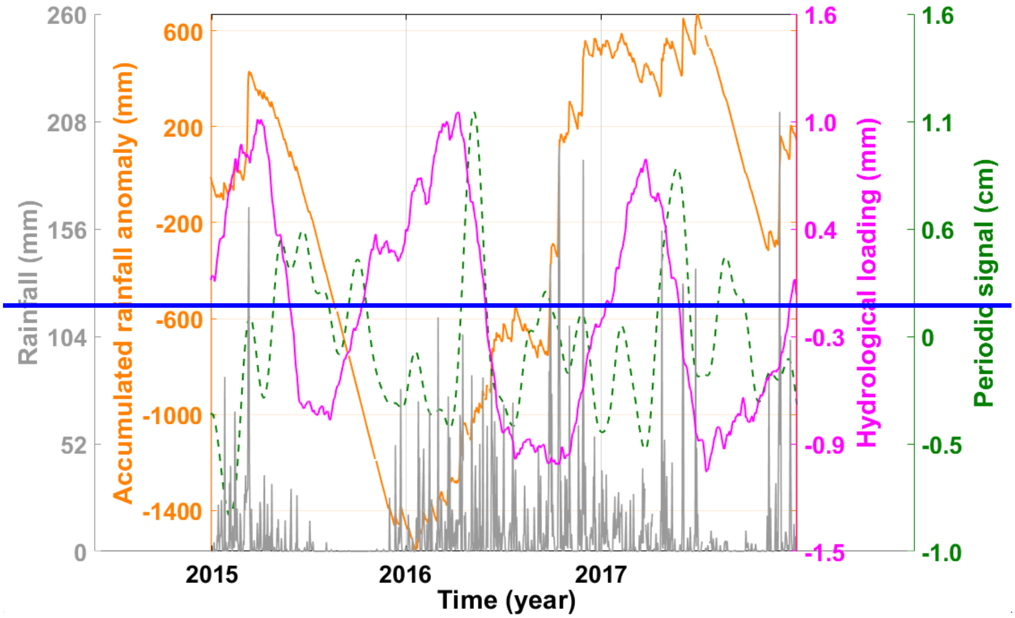


~~(a) XMIS station (2015-2017).~~

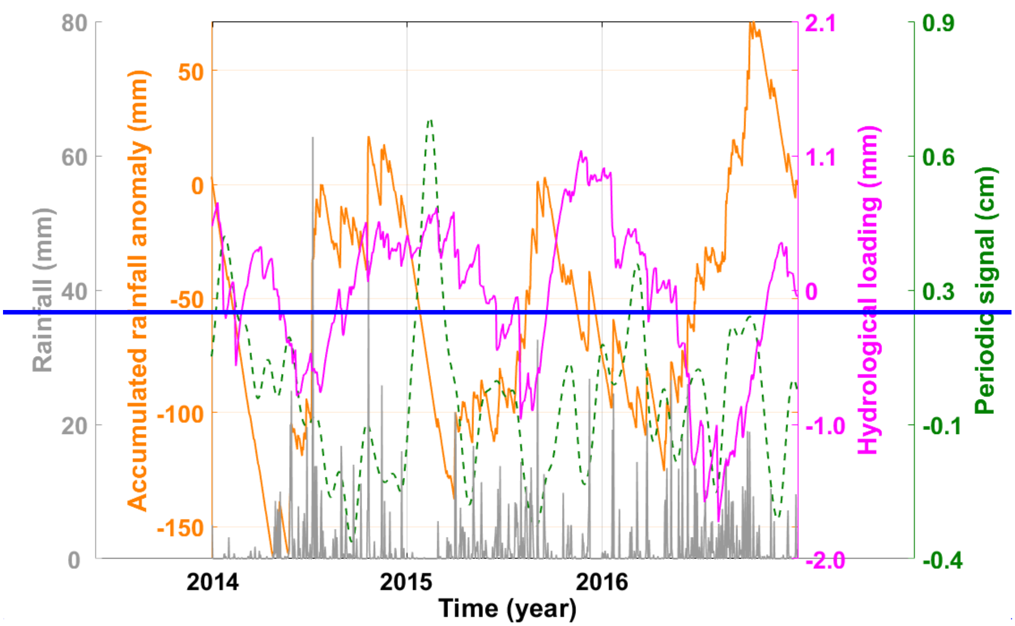


~~(b) ESPA station (2014-2016).~~

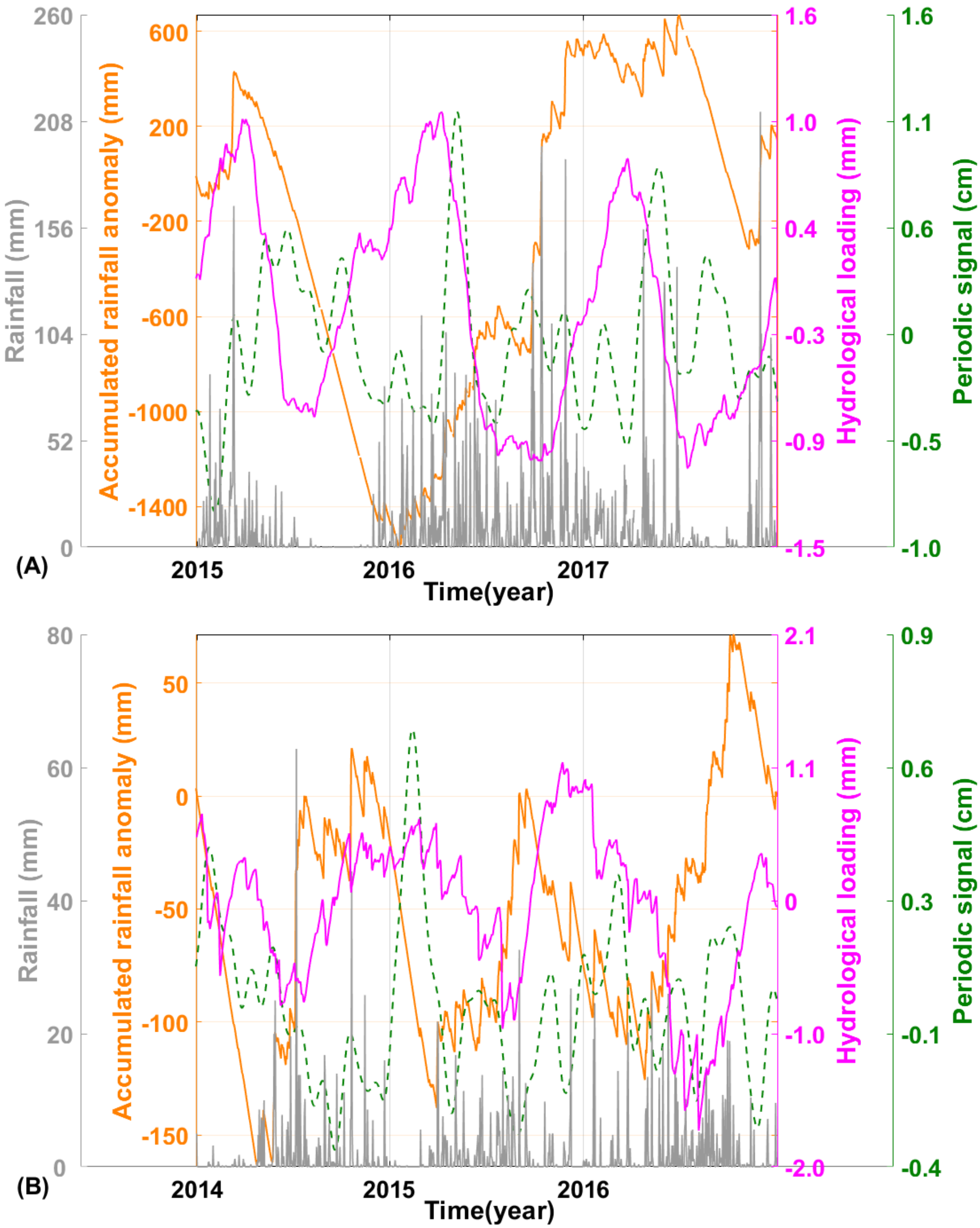


**Figure ~~14~~15: Abnormal periodic signal analysis at ~~(a)~~(A) XMIS station (2015-2017) and ~~(b)~~(B) ESPA station (2014-2016).**

## 5 Summary and conclusions

This paper employed the adaptive EEMD method for more efficient and accurate extraction of periodic signals. The simulations are conducted focusing on the inevitable missing data and offsets issues. The results revealed that with the missing data filled with the IEMD method, the adaptive EEMD method exhibits efficiency in signal extraction. As expected, with the percentage of missing data increases, the extracted periodic signals may gradually deviate from the true values. Specifically, for the random data missing, when the missing rate reaches 15%, RMSE and MAE show the rapid increases, at 0.11 and 0.05, respectively.For the consecutive data missing, when the missing lasts for one month, the increases in RMSE and MAE also reach their maximum values, at 0.32 and 0.06, respectively. Therefore, it is recommend that high accuracy could reach for the overall random missing rate below 15% and avoiding consecutive missing epochs exceeding 30 days when dealing with GNSS coordinate time series. Regarding the offset, it is apparent that correction beforehand is essential since RMSE and MAE are markedly reduced.That means offset detection and correction is also unignorable for the adaptive EEMD application. For the processing vertical component from 13 GNSS stations in Australia, adaptive EEMD shows its advantage over LS. The mean values for ~~correlation coefficient, spectral index~~ CC, RMSE, $\kappa$ and SNR for the adaptive EEMD are 0.36, 0.81, -0.18 and 0.48, respectively, while the mean values for LS are 0.27, 0.86, -0.50 and 0.23. Moreover, significance tests are conducted on the residuals , which further validates that annual signal still exist in the residuals for LS, while not for the EEMD. The periodic signals of the 13 investigated GNSS stations reflect the time-varying characteristics. It is found that the significant variations of the XMIS in 2016 and ESPA in 2015. Their ~~correlation coefficients~~ CC with hydrological loading are 0.50 and 0.57, respectively, indicating that hydrological loading is one primary factor contributing to the periodic variations.

In conclusion, this research highlights the advantages of the adaptive EEMD method for periodic signal extraction no matter in the synthetic or real GNSS coordinate time series analysis. The handling of missing data and offset are firstly comprehensively investigated, which provides helpful solution of preprocessing for EEMD. Furthermore, it reveals the time-varying characteristics of periodic signal, which is favorable in the subsequent trend ananalysis of the GNSS stations in SONEL network. Without doubt, the adaptive EEMD ~~is not limited~~ can also be applied not only to in the GNSS coordinate time series but also other geophysical data.

**Data availability**

~~Any data that support the findings of this study are included within the article.~~ The Australian region GNSS station data used in this study are all available from the Sonel website (https://www.sonel.org/spip.php?page=cgps&lang=en). The hydrological loading data is available from the EOST Loading Service (http://loading.u-strasbg.fr/listdata.php?dirn=dicf). Additionally, the daily rainfall time series can be obtained from the official website of the Australian Bureau of Meteorology (http://www.bom.gov.au/climate/).

## Author contributions

Weiwei Li: Conceptualization, Methodology, Investigation, Formal Analysis, Writing - Original Draft, Funding acquisition; Jing Guo: Data Curation, Formal Analysis, Writing - Original Draft.

## Competing interests

The authors declare that they have no competing interest.

## Acknowledgements

This research was funded by National Natural Science Foundation of China (41904011), Laoshan Laboratory (LSKJ202205104, LSKJ202205104_03) and Shandong Provincial Natural Science Foundation (ZR2019QD003).

## References

Agnieszka, W. and Dawid, K.: Modeling seasonal oscillations in GNSS time series with Complementary Ensemble Empirical Mode Decomposition, GPS. Solut., 26, 101, https://doi.org/10.1007/s10291-022-01288-2, 2022.

Abraha, K. E., Teferle, F. N., Hunegnaw, A. and Dach, R.: GNSS related periodic signals in coordinate time-series from Precise Point Positioning, Geophys. J. Int., 208, 1449-1464, https://doi.org/10.1093/gji/ggw467, 2017.

Bennett, R. A.: Instantaneous deformation from continuous GPS: Contributions from quasi-periodic loads, Geophys. J. Int., 174, 1052–1064, https://doi.org/10.1111/j.1365-246X.2008.03846.x, 2008.

Bos, M. S., Fernandes, R. M. S., Williams, S. D. P. and Bastos, L.: Fast error analysis of continuous GPS observations, J. Geodesy., 82, 157–166, https://doi.org/10.1007/s00190-007-0165-x, 2008.

Bos, M. S., Bastos, L. and Fernandes, R. M. S.: The influence of seasonal signals on the estimation of the tectonic motion in short continuous GPS time-series, J. Geodyn., 49, 205-209, https://doi.org/10.1016/j.jog.2009.10.005, 2010.

Bao, Z., Chang, G., Zhang, L., Chen, G. and Zhang, S.: Filling missing values of multi-station GNSS coordinate time series based on matrix completion, Measurement, 183, 109862, https://doi.org/10.1016/J.MEASUREMENT.2021.109862, 2021.

~~Blewitt, G. and Lavallée, D.: Effect of annual signals on geodetic velocity, J. Geophys. Res., 107, ETG 9-1-ETG 9-11, https://doi.org/10.1029/2001JB000570, 2002.~~

Blewitt, G., Kreemer, C., Hammond, W. C., Plag, H. P., Stein, S. and Okal, E.: Rapid determination of earthquake magnitude using GPS for tsunami warning systems, Geophys. Res. Lett., 33, L11309, https://doi.org/10.1029/2006GL026145, 2006.

Cai, F.: Study on global distribution laws and partial mechanisms of nonlinear variations of GNSS stations' coordinates, M.S. thesis, Strategic Support Force Information Engineering University, https://doi.org/10.27188/d.cnki.gzjxu.2020.000068, 2020. (in Chinese)

Chen, B., Bian, J., Ding, K., Wu, H. and Li, H.: Extracting seasonal signals in GNSS coordinate time series via weighted nuclear norm minimization, Remote. Sens-Basel., 12, 2027, https://doi.org/10.3390/rs12122027, 2020.

Calais, E., Gonzalez, O. F., Arango-Arias, E. D., Moreno, B., Palau, R., Cutie, M., Diez, E., Montenegro, C., Rodriguez Roche, E., Garcia, J., Castellanos, E. and Symithe, S.: Current deformation along the northern Caribbean plate boundary from GNSS measurements in Cuba, Tectonophysics, 868, 230068, https://doi.org/10.1016/j.tecto.2023.230068, 2023.

Costantino, G., Giffard-Roisin, S., Radiguet, M., Dalla Mura, M., Marsan, D. and Socquet, A.: Multi-station deep learning on geodetic time series detects slow slip events in Cascadia, Communications Earth & Environment, 4, 435, https://doi.org/10.1038/s43247-023-01107-7, 2023.

Cheng, J., Yu, D. and Yu Y.: Research on the intrinsic mode function (IMF) criterion in EMD method, Mech. Syst. Signal. Pr., 20, 817-824, https://doi.org/10.1016/j.ymssp.2005.09.011, 2006.

Dong, D., Fang, P., Bock, Y., Cheng, M. K. and Miyazaki, S.: Anatomy of apparent seasonal variations from GPS-derived site position time series, J. Geophys. Res., 107, ETG 9-1-ETG 9-16, https://doi.org/10.1029/2001JB000573, 2002.

~~Defraigne, P., Pinat, E. and Bertrand, B.: Impact of Galileo-to-GPS-Time-Offset accuracy on multi-GNSS positioning and timing, GPS. Solut., 25, 45, https://doi.org/10.1007/s10291-021-01090-6, 2021.~~

Davis, J. L., Wernicke, B. P. and Tamisiea, M. E.: On seasonal signals in geodetic time series, J. Geophys. Res., 117, B01403, https://doi.org/10.1029/2011JB008690, 2012.

Din, A. H. M., Zulkifli, N. A., Hamden, M. H. and Wan Aris, W. A.: Sea level trend over Malaysian seas from multi-mission satellite altimetry and vertical land motion corrected tidal data, Adv. Space. Res.-Series., 63, 3452-3472, https://doi.org/10.1016/j.asr.2019.02.022, 2019.

~~Feng, S, and Zheng Z.: Step offset recovery of GNSS continuous station and its effect on GNSS data processing, GNSS World of China, 38, 53-55+82, https://doi.org/10.13442/j.gnss.2013.05.010, 2013.~~

Gülal, E., Erdoğan, H. and Tiryakioğlu, İ.: Research on the stability analysis of GNSS reference stations network by time series analysis, Digit. Signal. Process., 23, 1945-1957, https://doi.org/10.1016/j.dsp.2013.06.014, 2013.

Griffiths, J. and Ray, J.: Impacts of GNSS position offsets on global frame stability, Geophys. J. Int., 204, 480-487, https://doi.org/10.1093/gji/ggv455, 2016.

Gazeaux, J., Williams, S., King, M., Bos, M., Dach, R., Deo, M., Moore, A. W., Ostini, L., Petrie, E., Roggero, M., Teferle, F. N., Olivares, G. and Webb, F. H.: Detecting offsets in GPS time series: First results from the detection of offsets in GPS experiment, J. Geoghys. Res.-Sol. Ea., 118, 2397-2407, https://doi.org/10.1002/jgrb.50152, 2013.

Horne, J. H. and Baliunas, S. L.: A prescription for period analysis of unevenly sampled time series, The Astrophysical Journal, 302, 757-763, 1986.

~~He, Y., Nie, G., Wu, S. and Li, H.: Comparative analysis of the correction effect of different environmental loading products on global GNSS coordinate time series, Adv. Space. Res Series., 70, 3594-3613, https://doi.org/10.1016/j.asr.2022.08.009, 2022.~~

Hetland, E. A. and Hager, B. H.: The effects of rheological layering on post-seismic deformation, Geophys. J. Int., 166, 277-292, https://doi.org/10.1111/j.1365-246X.2006.02974.x, 2006.

He, X., Montillet, J. P., Fernandes, R., Bos, M., Yu, K., Hua, X. and Jiang, W.: Review of current GPS methodologies for producing accurate time series and their error sources, J. Geodyn., 106, 12-29, https://doi.org/10.1016/j.jog.2017.01.004, 2017.

Huang, Y., Schmitt, F. G., Lu, Z. and Liu, Y.: Analysis of daily river flow fluctuations using empirical mode decomposition and arbitrary order Hilbert spectral analysis, Journal of Hydrology, 373, 103-111, https://doi.org/10.1016/j.jhydrol.2009.04.015, 2009.

Huang, N. E., Shen, Z., Long, S. R., Wu, M. C., Shih, H. H., Zheng, Q., Yen, N-C. Tung, C. C. and Liu, H. H.: The empirical mode decomposition and the Hilbert spectrum for nonlinear and non-stationary time series analysis, Proceedings of the Royal Society of London. Series A: mathematical, physical and engineering sciences, 454, 903-995, https://doi.org/10.1098/rspa.1998.0193, 1998.

Huang, N. E., Shen, Z. and Long, S. R.: A new view of nonlinear water waves: the Hilbert spectrum, Annu. Rev. Fluid. Mech., 31, 417-457, https://doi.org/10.1146/annurev.fluid.31.1.417, 1999.

Ide, S. and Tanaka, Y.: Controls on plate motion by oscillating tidal stress: Evidence from deep tremors in western Japan, Geophys. Res. Lett., 41, 3842-3850, https://doi.org/10.1002/2014GL060035, 2014.

~~Jiang, W. P., Li, Z., Liu, H. F. and Zhao, Q.: Cause analysis of the non-linear variation of the IGS reference station coordinate time series inside China, Chinese Journal of Geophysics, 56, 2228-2237, https://doi.org/10.6038/cjg20130710, 2013.~~

~~Jia, R. S., Zhao, T. B., Sun, H. M. and Yan, X. H.: Micro-seismic signal denoising method based on empirical mode decomposition and independent component analysis, Chinese Journal of Geophysics, 58, 1013-1023, https://doi.org/10.6038/cjg20150326, 2015.~~

Johnson, C. W., Lau, N. and Borsa, A.: An assessment of global positioning system velocity uncertainty in California, Earth and Space Science, 8, e2020EA001345, https://doi.org/10.1029/2020EA001345, 2021.

Kennedy, J., Dunn, R., McCarthy, M., Titchner, H. and Morice, C.: Global and regional climate in 2016, Weather, 72, 219-225, https://doi.org/10.1002/wea.3042, 2017.

Kopsinis, Y. and McLaughlin, S.: Improved EMD using doubly-iterative sifting and high order spline interpolation, Eurasip. J. Adv. Sig. Pr., 2008, 128293, https://doi.org/10.1155/2008/128293, 2008.

Klos, A., Olivares, G., Teferle, F. N., Hunegnaw, A. and Bogusz, J.: On the combined effect of periodic signals and colored noise on velocity uncertainties, GPS. Solut., 22, 1, https://doi.org/10.1007/s10291-017-0674-x, 2018.

Li, W.: Data adaptive analysis on vertical surface deformation derived from daily ITSG-Grace2018 model, Sensors, 20, 4477, https://doi.org/10.3390/s20164477, 2020.

Liu, X., Chen, W. and Mao, A.: An adaptive optimization EEMD method and its application in bearing fault detection, ResearchSquare [preprint], https://doi.org/10.21203/rs.3.rs-2615109/v1, 28 February 2023.

~~Li, M., Guo, S-W., Wei, N., Shi, C. and Gong, H-M.: Study on the draconitic year errors in GPS station coordinates, Progress in Geophysics, 33, 0473-0478, https://doi.org/10.6038/pg2018BB0145, 2018.~~

Li, W., Shen, Y.: Detection and analysis of velocity and amplitude changes in GNSS coordinate sequences, Journal of Tongji University, 42, 604-10, https://doi.org/10.3969/j.issn.0253-374x.2014.04.017, 2014. (in Chinese)

~~Łyszkowicz, A. and Bernatowicz, A.: Geocentric Baltic Sea level changes along the southern coastline, Adv. Space. Res-Series., 64, 1807-1815, https://doi.org/10.1016/j.asr.2019.07.040, 2019.~~

~~Manevich, A. I., Kaftan, V. I., Losev, I. V. and Shevchuk, R. V.: Improvement of the deformation GNSS monitoring network of the Nizhne-Kansk massif underground research laboratory site, Seismic Instruments., 57, 587-599, https://doi.org/10.3103/S0747923921050042, 2021.~~

Munekane, H.: Modeling long-term volcanic deformation at Kusatsu-Shirane and Asama volcanoes, Japan, using the GNSS coordinate time series, Earth. Planets. Space., 73, 192, https://doi.org/10.1186/s40623-021-01512-2, 2021.

~~Md Din, A. H., Zulkifli, N. A., Hamden, M. H. and Wan Aris, W. A.: Sea level trend over Malaysian seas from multi-mission satellite altimetry and vertical land motion corrected tidal data, Adv. Space. Res-Series., 63, 3452-3472, https://doi.org/10.1016/j.asr.2019.02.022, 2019.~~

Nishimura, T.: Pre-, co-, and post-seismic deformation of the 2011 Tohoku-oki earthquake and its implication to a paradox in short-term and long-term deformation, Journal of disaster research, 9, 294-302, https://doi.org/10.20965/jdr.2014.p0294, 2014.

Peng, W., Dai, W. J., Santerre, R., Cai, C. S. and Kuang, C. L.: GNSS vertical coordinate time series analysis using single-channel independent component analysis method, Physical and Engineering Sciences, 454, 903–995, https://doi.org/10.1007/s00024-016-1309-9, ~~1971~~2018.

~~Pan, Y., Ding, Hao., Li, J., Shum, C. K., Mallick, R., Jiao, J., Li, M. and Zhang, Y.: Transient hydrology-induced elastic deformation and land subsidence in Australia constrained by contemporary geodetic measurements, Earth. Planet. Sc. Lett., 588, 117556, https://doi.org/10.1016/j.epsl.2022.117556, 2022.~~

Press, W. H., Teukolsky, S. A., Vetterling, W. T. and Flannery, B. P.: Numerical Recipes: The Art of Scientific Computing, Third Edition, Cambridge University Press, ISBN9780521880688, 2010.

Qiu, X., Wang, F., Zhou, Y. and Zhou, S.: Iteration empirical mode decomposition method for filling the missing data of GNSS position time series, Acta. Geodyn. Geomater., 19, 271–279, https://doi.org/10.13168/AGG.2022.0012, 2022.

~~Qi, Y., W, L., Yang, Z. and Fu, Z.: Study on methods for improving EMD end effect, Modern Electronics Technique, 36, 50-52, https://doi.org/10.16652/j.issn.1004-373x.2013.22.029, 2013.~~

Rodionov, N. S.: A sequential algorithm for testing climate regime shifts, Geophys. Res. Lett., 31, 9, https://doi.org/10.1029/2004GL019448, 2004.

Ray, J., Altamimi, Z., Collilieux, X. and Van Dam, T.: Anomalous harmonics in the spectra of GPS position estimates, GPS. Solut., 12, 55-64, https://doi.org/10.1007/s10291-007-0067-7, 2008.

Ran, J., Bian, J., Chen, G., Zhang, Y. and Liu, W.: A truncated nuclear norm regularization model for signal extraction from GNSS coordinate time series, Adv. Spa. Pace. Res., 70, 336-349, https://doi.org/10.1016/j.asr.2022.04.040, 2022.

~~Shu, Y.: Comparative analysis on outlier elimination methods for GPS coordinate time series, Journal of Navigation and Positioning, 9, 79-85, https://doi.org/10.16547/j.cnki.10-1096.20210412, 2021.~~

Scaramuzza, S., Dach, R., Beutler, G., Arnold, D., Sušnik, A. and Jäggi, A.: Dependency of geodynamic parameters on the GNSS constellation, J. Geodesy., 92, 93-104, https://doi.org/10.1007/s00190-017-1047-5, 2017.

Shen, Y., Li, W., Xu, G. and Li, B.: Spatiotemporal filtering of regional GNSS network's position time series with missing data using principle component analysis, J. Geodesy., 88, 1-12, https://doi.org/10.1007/s00190-013-0663-y, 2014.

Sorin, N., NorbertSzabolcs, S., Ahmed, E., Michal, A., Zinovy, M., Ilie, N. E., Jacek, K. and Kamil, M.: Implication between geophysical events and the variation of seasonal signal determined in GNSS position time series, Remote. Sens-Basel., 13, 3478-3478, https://doi.org/10.3390/RS13173478, 2021.

Singh, A., Reager, J. T. and Behrangi, A.: Estimation of hydrological drought recovery based on precipitation and Gravity Recovery and Climate Experiment (GRACE) water storage deficit, Hydrol. Earth. Syst. Sc., 25, 511-526, https://doi.org/10.5194/hess-25-511-2021., 2021.

Su, L., Zhai, H., Wang, Q. and Tian, X.: Detecting offsets in GPS coordinate time series based on SSA method, Journal of Geodesy and Geodynamics, 43, 464-466, https://doi.org/10.14075/j.jgg.2023.05.005, 2023. (in Chinese)

Tobita, M.: Combined logarithmic and exponential function model for fitting postseismic GNSS time series after 2011 Tohoku-Oki earthquake, Earth. Planets. Space., 68, 1-12, 2016.

Tehranchi, R., Moghtased-Azar, K. and Safari, A.: A new statistical test based on the WR for detecting offsets in GPS experiment, Earth and Space Science, 7, e2019EA000810, https://doi.org/10.1029/2019EA000810, 2020.

Van Dam, T., Wahr, J., Milly, P. C. D., Shmakin, A. B., Blewitt, G., Lavallée, D. and Larson, K. M.: Crustal displacements due to continental water loading, Geophys. Res. Lett., 28, 651–654, https://doi.org/10.1029/2000GL012120, 2001.

Wang, J., Ding, K., Sun, H., Zhang, G. and Chen, X.: Noise reduction and periodic signal extraction for GNSS height data in the study of vertical deformation, Geodesy and Geodynamics, 14, 573-581, https://doi.org/10.1016/j.geog.2023.07.002, 2023.

Wang, L. and Herring, T.: Impact of estimating position offsets on the uncertainties of GNSS site velocity estimates, J. Geophys. Res-Sol. Ea., 124, 13452-13467, https://doi.org/10.1029/2019JB017705, 2019.

Wu, Z. and Huang, N. E.: Ensemble empirical mode decomposition: a noise-assisted data analysis method, Advances in Adaptive Data Analysis, 1, 1-41, https://doi.org/10.1142/S1793536909000047, 2009.

Willen, M. O., Horwath, M., Groh, A., Helm, V., Uebbing, B. and Kusche, J.: Feasibility of a global inversion for spatially resolved glacial isostatic adjustment and ice sheet mass changes proven in simulation experiments, J. Geodesy., 96, 75, https://doi.org/10.1007/S00190-022-01651-8, 2022.

Wang, K., Jiang, W., Chen, H., An, X., Zhou, X., Yuan, P. and Chen, Q.: Analysis of seasonal signal in GPS short-baseline time series, Pure. Appl. Geophys., 175, 3485–3509, https://doi.org/10.1007/s00024-018-1871-4, 2018.

Wu, F. and Qu, L.: An improved method for restraining the end effect in empirical mode decomposition and its applications to the fault diagnosis of large rotating machinery, J. Sound. Vib., 314, 586-602, https://doi.org/10.1016/j.jsv.2008.01.020, 2008.

~~Xu, F.: GNSS monitoring data processing based on ensemble empirical mode decomposition method, Geomatics Technology and Equipment, 24, 102-109, https://doi.org/10.20006/j.cnki.61-1363/P.2022.03.020, 2022.~~

~~Yi, W. H., Yan, L., Wang, Z. H., Yang, J. H. Tao, T. J. and Liu, L. S.: Geotechnical engineering blasting: a new modal aliasing cancellation methodology of vibration signal de-noising, Earthq. Eng. Eng. Vib., 21, 313-323, https://doi.org/10.1007/s11803-022-2094-3, 2022.~~

~~Zheng, J.: Experimental study on the method of IMF component judgment criterion in Empirical Mode Decomposition, Journal of Geomatics, 46 ,33-37, https://doi.org/10.14188/j.2095-6045.2018391, 2021.~~

~~Zhang, J., Wang, X. and Hu X.: Analysis of GPS stations' time series based on PCA method, Journal of Geodesy and Geodynamics, 39, 613-619, https://doi.org/10.14075/j.jgg.2019.06.012, 2019.~~

~~Zhang, J., Yan, R. Q. and Gao, R. X.: Ensemble Empirical Mode Decomposition for machine health diagnosis, Key. Eng. Mat., 413, 167-174, https://doi.org/10.4028/www.scientific.net/KEM.413-414.167, 2009.~~

Zaccagnino, D., Vespe, F. and Doglioni, C.: Tidal modulation of plate motions, Earth-science reviews, 205, 103179, https://doi.org/10.1016/j.earscirev.2020.103179, 2020.

Zhou, X., Yang, Y., Chen, Q., Fan, W. and Ma, Y.: A robust trend estimator for GNSS time series in the presence of complex periodicity and its evaluation on multi-source products of IGS and IGMAS, GPS. Solut., 26, 103, https://doi.org/10.1007/s10291-022-01271-x, 2022.